Perturbations of Ribosomal Protein Expression Reveal Overlapping Gene Networks between *Drosophila* Minutes and Human Cancer

Jai A Denton[1,*,#], Mariana Velasque[1,*] & Floyd A Reed[2]

[1] Genomics & Regulatory Systems Unit, Okinawa Institute of Science & Technology, 1919-1 Tancha, Okinawa, Japan
[2] School of Life Sciences, University of Hawaiʻi at Mānoa, 2538 McCarthy Mall, Honolulu, HI 96822

[*] These authors contributed equally
[#] Corresponding author: jai.denton@oist.jp

Abstract
Ribosomal proteins (RPs) are critical to all cellular operations through their key roles in ribosome biogenesis and translation, as well as their extra-ribosomal functions. Although highly tissue- and time-specific in expression, little is known about the macro-level roles of RPs in shaping transcriptomes. A wealth of RP mutants exist, including the *Drosophila melanogaster* Minutes, with RP encoding genes that vary from greatly under-expressed to greatly over-expressed. Leveraging a subset of these mutants and using whole-body RNA sequencing, we identified the RP macro transcriptome and then sought to compare it with transcriptomes of pathologies associated with failures of ribosomal function. Gene-based analysis revealed highly variable transcriptomes of RP mutations with little overlap in genes that were differentially expressed. In contrast, weighted gene co-expression network analysis (WGCNA) revealed a highly conserved pattern across all RP mutants studied. When we compared network changes in RP mutants, we observed similarities to transcriptome alterations in human cancer, and thus confirming the oncogenic role of RPs. Therefore, what may appear stochastic at the individual gene level, forms clearly predictable patterns when viewed as a whole.

Keywords: Minute; Ribosomal protein; RNA Sequencing; Transcriptome; Cancer

Introduction

Gene networks are typically more than the sum of their parts. As new components are added to a network, complexity can increase exponentially, such that it is difficult to predict or even assess the reverberations the consequences small changes have throughout entire networks (Crow et al., 2019). Therefore when examining changes brought on by the modification of a single network component, it is important to examine not just how other single components are affected but how networks themselves change. As networks grow in size and influence a greater number of cellular processes, this becomes more critical.

Ribosomal proteins (RPs) are a diverse group of highly conserved proteins that are central to ribosome biogenesis. Given the dependency of normal cellular function on rapid and accurate protein production, it is unsurprising that mutations in RP-encoding genes are highly deleterious, resulting in a variety of adverse outcomes (Wang et al., 2015; Yassin et al., 2005). Thus, homozygous deletion or mutation of RPs is typically lethal (McGowan et al., 2008), whereas heterozygous RP mutations are typically haploinsufficient with a fitness cost (Kim et al., 2010; Marygold et al., 2007; Weijers et al., 2001; Zheng et al., 2016). In addition to their role in ribosome biogenesis and function, some RPs have important extra-ribosomal activities (Warner and McIntosh, 2009). Their mis-expression has been detailed in numerous aberrant cellular processes. In recent years, RPs have been shown to participate in stress responses, nucleolar integrity, cell cycle control, cell proliferation, genome integrity, telomere length and cell death (Abdulkina et al., 2019; Lai et al., 2009; Moin et al., 2016; Nicolas et al., 2016). Thus, ribosome biogenesis is highly dose-dependent, with small changes impacting numerous cellular processes.

Due to this diverse array of cellular functions, RP mutations potentiate cancer. Suboptimal ribosome biogenesis, or incorrect function of RPs generally result in oncogenesis (Lai et al., 2009; Oršolić et al., 2020), whereas their normal functioning is tumor-suppressive (Amsterdam et al., 2004; Fancello et al., 2017). As such, RP mutations are associated with diverse cancers (De Keersmaecker et al., 2013; Rao et al., 2012). Moreover, hyperactivation of ribosome biogenesis is also frequently seen in cancer cells (Dolezal et al., 2018). Impaired ribosome biogenesis arrests cell cycle progression in a p53-dependent manner (Volarević et al., 2000; Pestov et al., 2001). This occurs through RP-mediated stabilization of p53, with critical involvement of RpL5 and RpL11 (Bursać et al., 2012). Mutant forms of these two RPs have been documented in many cancers (Dong et al., 2017). In addition, RpL22, RpL10, RpS15, RpS20 and RpL5 are also mutated in diverse human cancers. Moreover, patients with Diamond-Blackfan anemia, which results from mutations in a wide range of RPs, are at a higher risk of developing cancer (Boria et al., 2010). Thus, either directly or indirectly, by virtue of being highly pleiotropic in cellular processes, RPs are critical in oncogenesis.

RPs in *Drosophila melanogaster* predominantly include a class of mutants known as the Minute loci (Bridges et al., 1923; Kongsuwan et al., 1985; Lambertsson, 1998; Marygold et al., 2007). First described in *D. melanogaster* almost a century ago (Bridges et al., 1923), the Minute loci were originally named for their resulting smaller bristles. In addition to thinner bristles, Minutes bearing flies exhibit delayed development, lower viability and fertility, and altered body size (Bridges et al., 1923; Marygold et al., 2007).

These are dominant phenotypes due to haploinsufficiency of RPs, and with rare exception, are homozygous lethal (Marygold et al., 2007).

Despite comprehensive study of RPs and Minute loci in *D. melanogaster*, regulatory response and cellular outcomes remain little understood. For instance, despite the pleiotropic nature of RPs, it is unknown whether disruption of RPs causes a standard cellular or a transcriptomic response. Recent work identified XRP1, a DNA-binding protein involved in genome stability, as essential to regulate the cellular response to aberrant RpS3 and RpS17 expression in *D. melanogaster* (Lee et al., 2018). It was also shown that mutations in the RpS3 or mahjong genes activate Toll and oxidative stress pathways and the Nrf2 (cnc) stress factor (Kucinski et al., 2017). Given the pleiotropic and variable nature of RP disruptions, further analysis is required to determine whether RPs share a transcriptomic response or if these mutations shape the transcriptome on an individual basis.

In the present study, we have investigated whether there are consistent single gene and network transcriptomic responses to RP mutations in *D. melanogaster* using whole-body RNA sequencing data from 7 RP mutant lines. We have selected Minute loci arising from *P*-element disruption of RP-encoding genes, identified on the basis of their phenotypes and the location of *P*-element genomic insertions. Furthermore, we sought to contextualise transcriptomic responses using available transcriptomic data from cancer cells.

Results

Genomic Locations of Ribosomal Protein-Encoding Genes

RPs are not clustered within the genome. If the distribution of RPs in the genome were random, it should result in exponentially distributed distances between adjacent RPs. However, we found that their distribution was consistent with non-clustered, essentially random placement in the genome (n=86, KS-test D=0.1121, P=0.2134) (Figure 1).

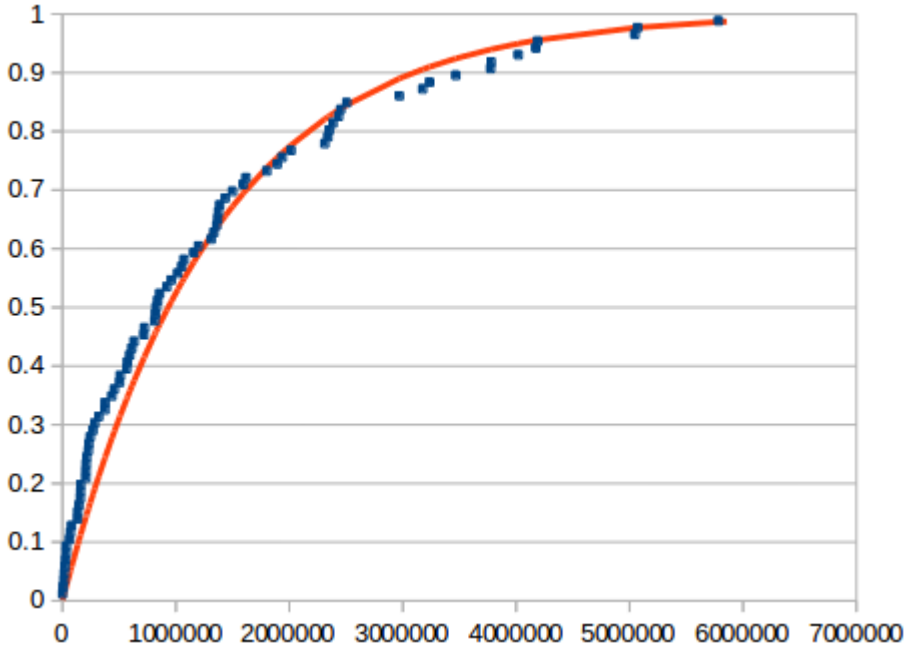

Figure 1 - RPs are distributed essentially randomly in the *Drosophila* genome. The cumulative fraction shown in blue and the theoretical exponential curve based on a Poisson process is plotted for comparison in red. RP placement is random (n=86, KS-test D=0.1121, P=0.2134).

Aberrant Expression of RPs

RP mutants were generated using *P*-element mutagenesis and have been previously confirmed as Minutes via phenotypic screens (Marygold et al., 2007). We detected aberrant expression of target RPs in five of seven Minute *P*-element mutagenesis lines used when compared to an unmutated control (adj-p<0.05) (Table 1). RNA sequencing was employed to identify transcriptomic changes in these haploinsufficient heterozygous mutants. RNA sequencing was successfully performed on single flies from seven RP mutagenesis lines (Materials & Methods). With the exception of RpS19b, each line displays reduced expression of the target RP, ranging from -0.03 to -0.91-fold ($\log_2$)change (Table 1). However, RpS19b was upregulated almost 5-fold ($\log_2$). As the P-element insertion for the RpS19b mutant is 34 bp upstream from the start codon, the inserted promoter is likely driving the over expression (FlyBase - FBrf0230790/FBti0181318). Although previous research confirmed the Minute phenotype and characterised the genome insertion (Marygold et al., 2007), our analysis did not detect a significant change in the target RPs, RpL3 or RpL30 (adj-p > 0.05). These were also the two smallest expression changes, 0.03 and 0.17, respectively. However, despite the absence of a statistically significant reduction in expression, RpS19b, RpL3,

and RpL30 are included in the analysis as they are confirmed mutants with characterised phenotypes.

Table 1 - Ribosomal Protein Gene Expression. Expression values for each of the affected ribosomal protein-encoding genes in their respective mutant backgrounds compared to an control. For example, Strain RpL14 contains expression data for RpL14. Each transcript had comparatively lower expression, consistent with a knockdown, except RpS19, which had considerably higher expression. Neither RpL3 nor RpL30 had significantly different expression (adj-p > 0.05). The strain names refers to gene affected but is only a single allele (Table 7)

Strain	Gene ID	log2-Fold Change	p-adj
RpS13	*FBgn0010265*	*-0.909*	*<0.001*
RpL24_like	*FBgn0037899*	*-0.475*	*0.015*
RpL3	*FBgn0020910*	*-0.034*	*0.807*
RpL30	*FBgn0086710*	*-0.174*	*0.157*
RpS19b	*FBgn0039129*	*4.765*	*<0.001*
RpL14	*FBgn0017579*	*-0.4833*	*<0.001*
RpL19	*FBgn0002607*	*-0.903*	*<0.001*

The Minute Transcriptome

There is no strong shared transcriptomic response between Minute mutations. Each of the Minute strains tested displayed a considerable number of genes that were differentially expressed relative to a control strain (adj-p <0.05) (Supplementary Figure 1, Table 2). The data show large numbers of differentially expressed genes, typically with small magnitude changes. There is also considerable variation in the number of differentially expressed genes, with RpL24-like having 3350 and RpS13 having 469. As such there is unlikely to be a clearly defined core of genes among RP mutants.

Table 2 - Differentially expressed genes. The number of differentially expressed (DE) genes in each treatment (strain). The strain names refers to gene affected but is only a single allele (Table 7)

Strain	DE Genes
RpS13	*469*
RPL14	*772*
RPL19	*1196*
RpL30	*1903*
RpL3	*2128*
RpS19b	*2880*
RpL24-like	*3350*

There are only 18 genes differentially expressed across all RP mutants (Table S1). Even with the removal of RpS13, which raises shared differentially expressed genes to 67, a clearly defined transcriptomic response is lacking. In the absence of a single core transcriptome, we explored the possibility of overlapping groups of differentially expressed genes. This analysis shows considerable overlap between various groups

(Figure 2). For example, RpS30, RpS3, RpS19b and RpL24-like share 441 differentially expressed genes.

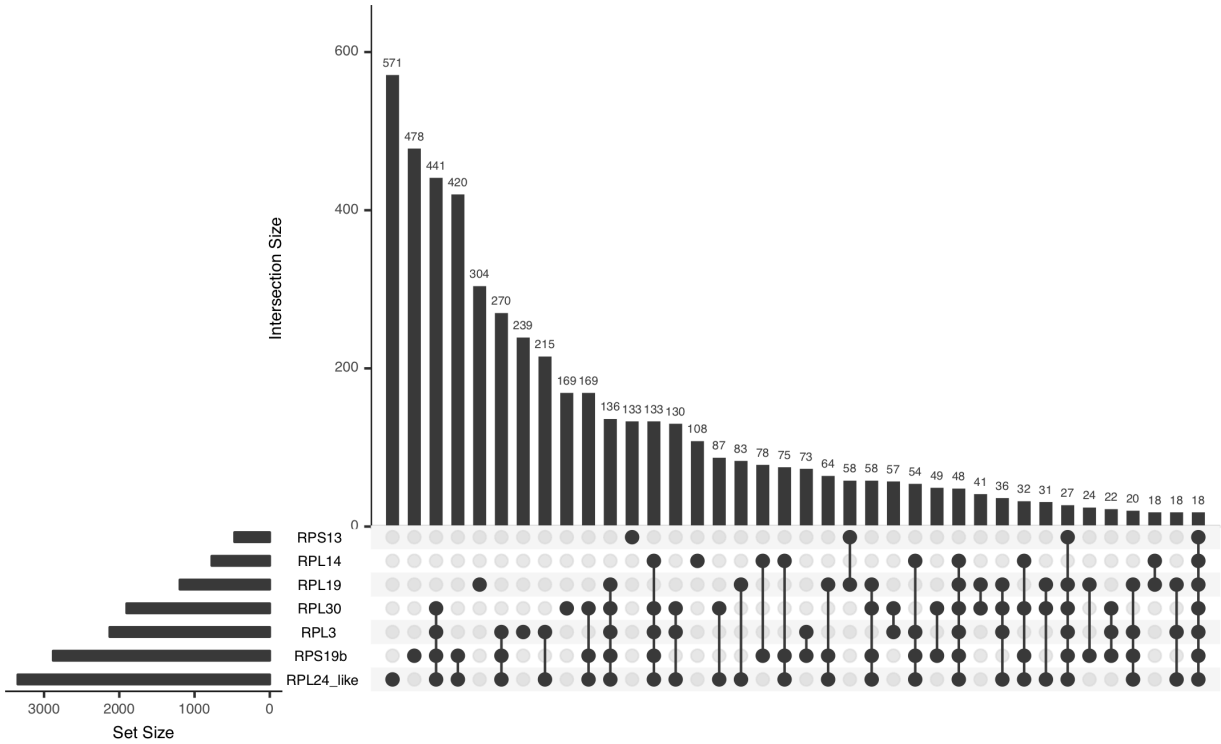

Figure 2 - UpSetR diagram detailing overlapping differentially expressed genes between ribosomal protein (RP) mutants. A Venn diagram-like representation of differentially expressed (DE) genes exhibiting statistically significant changes (adj p-value <0.05). Set Size denotes the total number of DE genes. Linked dots and corresponding column indicate the number of DE genes shared between those RP mutants. Single dots indicate the number of DE genes unique to the RP mutant.

Single-Gene Misregulation

As no clear pattern of expression was observed across all mutants in response to mutations in RP-encoding genes, both previously identified regulatory genes and markers for implicated pathways were examined.

Previous work identified XRP1 and IBRBP1 as being upregulated in response to aberrant RP expression (Lee et al., 2018; Blanco et al., 2020). However, we were unable to identify XRP1 or IBRBP1 as a clear marker. Only in the RpS13 line was XRP1 upregulated (adj p-value < 0.05) (Table 3). IBRPB1 was not upregulated in any line, although it was downregulated in RpL24-like (Table 3).

As several pathways controlled by a handful of key genes have also been implicated in the cellular response to RP mutations, a candidate gene-based approach was undertaken. Of the 20 candidate genes examined, only asp, CycB3, pik92e, ask1 & bsk were differentially expressed in four or more of the RP mutants (Supplementary Table S2).

Table 3 - XRP1 / IRBP1 Expression in each RP mutant strain.

	XRP1		IRBP1	
	log2 - Fold Change	**p-adj**	**log2-Fold Change**	**p-adj**
RpS13	0.648	0.0346	0.223	0.416
RpL24-like	-0.1609	0.5723	-0.364	0.038
RPL3	-0.1816	0.5448	-0.152	0.446
RPL30	-0.2951	0.2863	-0.150	0.447
RpS19b	-0.3835	0.1371	-0.275	0.124
RpL14	-0.453	0.1181	-0.100	0.656
RpL19	0.0911	0.8155	-0.012	0.969

Minute Gene Ontology

Although there are very few differentially regulated core genes, there is a large core of gene ontology (GO) categories shared among all seven mutant lines. We classified differentially expressed genes for each of the mutant lines based on biological function GO. 138 GO categories were shared by all mutant lines (Supplementary Table S3). These categories included RNA processing, translation, and programmed cell death. Moreover, using pairwise comparisons, it is clear that there is considerable overlap in the biological processes affected by RP mutations (Figure 3). However, GO analysis based on differentially expressed genes can be limited especially when large numbers of genes are differentially expressed (Boyle et al., 2017). Thus we employed network analysis to provide a more accurate view of how the transcriptome is shaped by RP mutations.

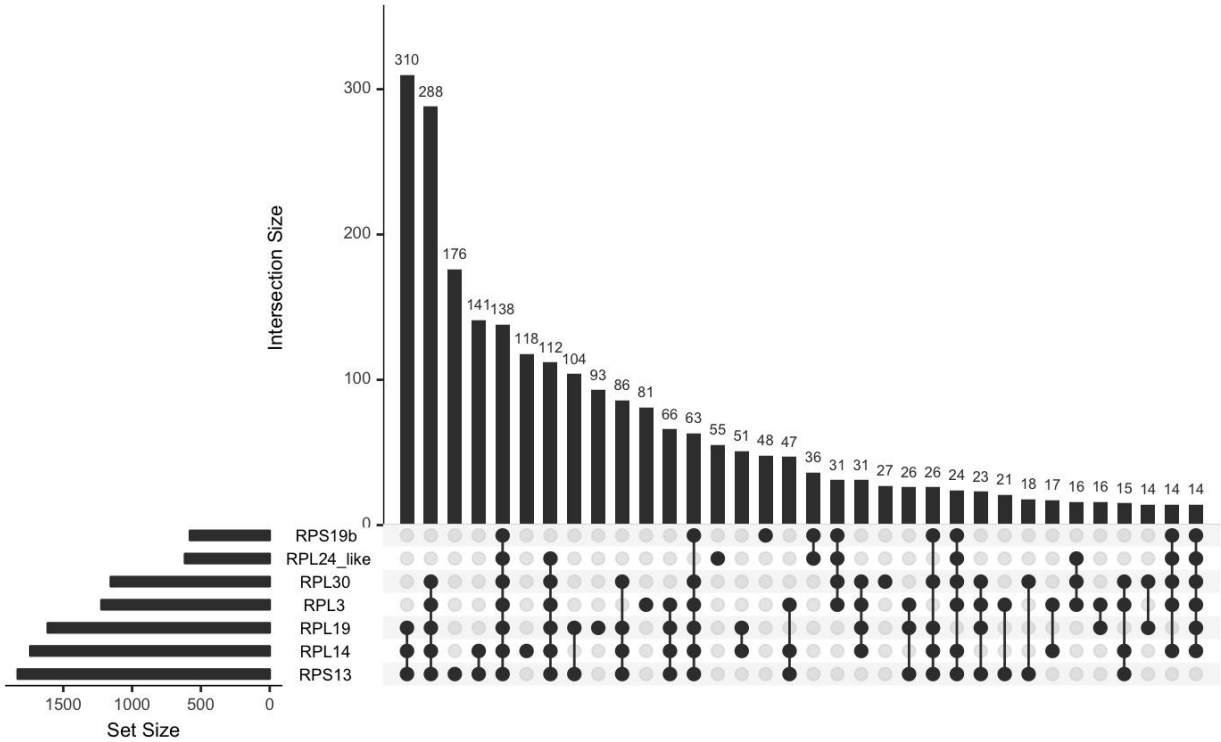

Figure 3 - UpSetR diagram detailing overlapping biological process gene ontology (GO) categories of differentially expressed genes in each of the RP mutants. A Venn diagram-like representation of GO categories for the differentially expressed (DE) genes (adj p-value <0.05). Set Size denotes the total number of GO categories. Linked dots and the corresponding column indicate the number of GO categories shared between those RP mutants. Single dots indicate the number of GO categories unique to that specific RP mutant.

RP Network Analysis

Genes are not independent. Their activation and expression depend on a series of interactions with other genes and pathways. Genes with similar biological functions tend to be regulated by the same transcription factor and, overall, have similar expression profiles (Weirauch, 2011). Therefore, associations can be identified by clustering groups of genes with similar expression (i.e. co-regulated) into modules, improving functional genome annotation using the *guilt-by-association principle* (Wolfe et al., 2005). Similarly, differences in network co-expression patterns between two groups or treatments can be used to indicate gene clusters involved in a particular pathway. Differential network analysis, where differences in gene co-expression between two data sets can be used to identify condition-associated pathways, leverages these co-expression patterns and is an alternative to typical differential gene expression analysis (Bhuva et al., 2019; Hsiao et al., 2016).

We first explore the differences between each RP mutant strain and the control and identify structural changes in pathways associated with ribosome biogenesis dysregulation (RP Differential Network Analysis). Although knowledge of changes in ribosomal pathway in Minutes are crucial to understand how ribosomes are regulated, the information on the whole cluster (differentially or not differentially co-expressed) is missing. Therefore, we also attempted to identify the ribosomal hub modules , by identifying clusters of genes co-expressed in each Minute strain (RP Weighted Gene Co-expression Network Analysis).

RP Differential Network Analysis

The Differential Network Analysis (Materials & Methods) was used to identify differences in pathways between Minutes and control were tested via permutation. A total of 6004 unique genes were found to be differentially co-expressed in at least one RP mutant strain (Table 4). The data show a large number of differentially co-expressed (DCE) genes within the ribosomal pathway. Although all networks have shown high connectivity between DCE genes, there is a large variance in magnitude across the DCE genes and large core of shared genes (61). Similar to the DE analysis, we were unable to identify XRP1 or IBRBP1 as part of the ribosomal network.

Although we identified this 61 gene core, no significant gene ontology categories were shared between all strains. Differentially co-expressed genes were classified based on the on biological function GO and a total of 171 GO (Figure 4) categories were present in at least one of the mutant lines (Supplemental material S2)

Table 4 - Differentially co-expressed genes. The number of differentially co-expressed (DCE) genes in each treatment (strain) pathway. The strain names refers to gene affected but is only a single allele (Table 7)

Strain / Gene	DCE Genes
RpL3	2640
RpL14	1426
RpS13	1143
RpS19b	3203
RpL19	1874
RpL24-like	2580
RpL30	3119

RP Weighted Gene Co-expression Network Analysis

The weighted gene co-expression network analysis (WGCNA) (Materials & Methods) is a systematic biological method used to describe patterns of gene associations between samples and treatment groups. It uses expression of thousands of genes to construct co-expression modules related to a phenotype or treatment group. Thus, it has been extensively used in genome studies to identify gene sets of interest or gene networks (Langfelder and Horvath, 2008).

We attempted to understand how changes in RP expression affects modules through changes in gene clustering. In other words, we investigated whether RP expression of mutants had a different clustering pattern when compared to controls (Spradling et al., 1999). The transcriptomic network of each RP mutant was contrasted with that of the wild type. With network construction, we measured intramodular gene connectivity between mutants, selecting highly connected genes, defined as RP hub genes. These hub genes were highly connected in their respective RP modules and are likely to serve critical functions in regulating ribosomal activity. Thus, for each mutant, we identified hub genes and their patterns of expression, identifying a list of differentially

expressed genes (see S2 Supplemental Materials for a full list). We also investigated whether the expression of such RP hub genes was conserved across experimental groups.

Module preservation is a measure of how gene clusters (small subsets within a network) from two different sets of data have similar expression profiles. Preservation is measured using Zsummary results and respective p-values. A Zsummary statistic of >10 is considered strongly similar, >5 moderately similar and <2 as dissimilar. Our Zsummary scores (>10) indicate stronger evidence that a module is well preserved across all RP mutants (Table 5). p-values for WGCNA Module preservation analysis ranged between 5.89E-12, for RpL3 / RpS13, to 1.04E-78, for RpS19b / RPL30. This suggests a well conserved transcriptomic response among all RP mutants. For example, within the RpL3 mutant transcriptome, the module containing all genes that grouped with RpL3 was compared to the module grouping all RpL14-responsive genes from the RpL14 mutant.

Table 5 - WGCNA Module Preservation. The reported Zsummary, shown in blue, and p-values, shown in yellow, of module correlations between each mutant strain. This is a pairwise comparison between a pair of modules containing the strain-specific RP mutation (e.g., *RpL3*-containing module in the RpL3 strain compared against the *RpL14*-containing module in the RpL14 strain).

	RpL3	Rpl14	RpS13	Rp19b	RpL19	RpL24-like	RpL30
RpL3		<0.0001	<0.0001	<0.0001	<0.0001	<0.0001	<0.0001
Rpl14	12.6465		<0.0001	<0.0001	<0.0001	<0.0001	<0.0001
RpS13	13.3311	17.1543		<0.0001	<0.0001	<0.0001	<0.0001
Rp19b	21.5842	16.7581	10.8456		<0.0001	<0.0001	<0.0001
RpL19	17.4687	17.5810	14.9769	19.5649		<0.0001	<0.0001
RpL24-like	22.1592	15.0877	11.2195	24.7626	16.9910		<0.0001
RpL30	22.0449	16.4723	13.3747	26.2302	20.2664	24.6987	

Network analysis not only showed that components of target modules were conserved, but highlighted the preserved nature of the RP gene network, suggesting a common activation pathway (see S2 Supplemental Materials for a full list of shared genes). Using GO analysis, we also investigated biological processes of RP hub genes (Supplementary Figures 1-7). However, we did not find any significantly enriched group in our analysis. Furthermore, the module preservation analysis also revealed that the majority of genes present on the network are shared by multiple RP modules.

The high degree of module preservation between RP mutant strains means that direct comparisons can be conducted between these strains and other transcriptomic datasets with proposed RP-driven effects. This allows us to seperate transcriptomes that are a product of RP-based changes from those wherein RPs are affected as a result.

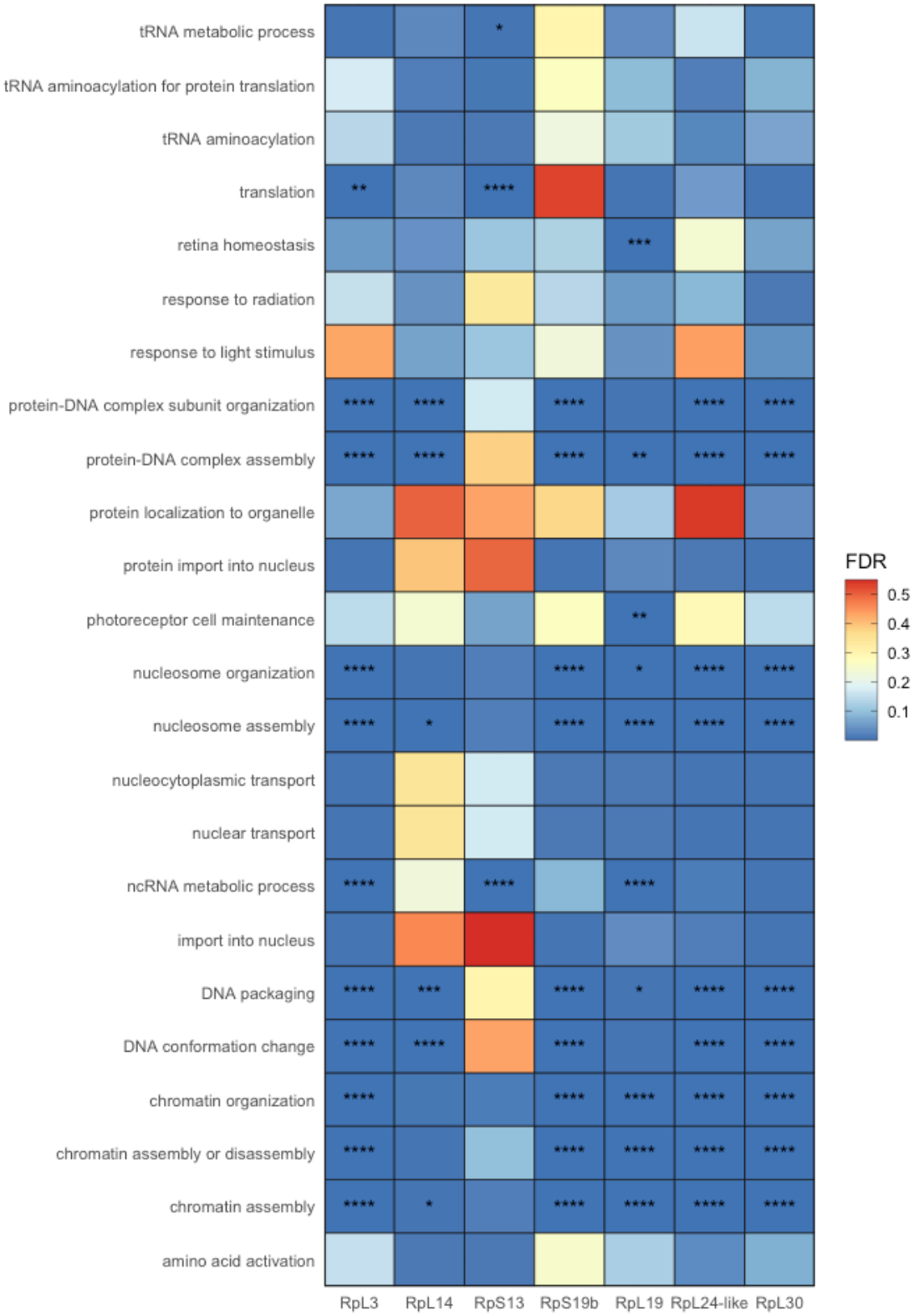

Figure 4 - List of Gene Ontology (GO) terms that were significantly enriched among differentially co-expressed genes in RP mutant strains. The gradient (red to blue) shows the false discovery rate for each GO term. Asterisks denote statistically significant enrichment ($p < 0.05$), double, triple and four asterisks denote significant enrichment ($p < 0.01$, $p < 0.001$ and $p < 0.0001$ respectively).

RPs, Cancer & Zika Virus - Comparative WGCNA

As RPs are highly conserved across the Eukaryota and glioblastoma and breast cancer have been previously attributed to disruption of RP genes (Penzo et al., 2019), we compared preservation levels between RP hub genes and their human counterparts. Moreover, although aberrant RP activity has been implicated in Zika virus infections, it has been proposed the aberrant activity is a response to rather than a driver of changes in the tissue of Zika virus infected individuals (Hetman and Slomnicki, 2019; Slomnicki et al., 2017). Therefore, cancer and Zika transcriptomic datasets can be contrasted with RP mutants to determine the accuracy of these hypotheses.

After constructing gene co-expression modules and identifying hub genes for each RP mutant, we determined the level of preservation between each RP mutant and cancer or Zika datasets (Figure 5; Materials and Methods). This was achieved via comparison of the *D. melanogaster* (17,559 genes) and *Homo sapiens* (56,212 genes) data sets to identify homologues (8,446 genes; Figure 5b). As a conservative direct comparison, these 8,446 homologous genes were used for subsequent WGCNA analysis to determine whether mutations in RPs induce expression changes resembling those in glioblastoma or breast cancer, or Zika virus-infected neuroblastoma cells.

As in the RP Network Analysis, we employed the modulePreservation function in the WGCNA package, using two network-based composite preservation statistics (Zsummary). We found eight RP modules and 6,729 unique genes having well-defined human counterparts (5 modules and 4,392 genes in glioblastoma and 3 modules and 5,730 genes in breast cancer were highly preserved; Table 6). Like cancer, Zika virus also controls its translation activity through internal ribosomal entry sites, altering translation of ribosomal subunits (Song et al., 2019). Thus, we also compared the preservation of RP hub genes between mutants and the Zika virus infection profile. We did not find any evidence that RP networks are well preserved between mutants and Zika virus infection (Table 6).

We then estimated intramodular connectivity (i.e. connectivity between genes in the same module) of conserved RP modules. Intramodular connectivity was then used to visualise connectedness of RP-hub genes in Minutes (Figure 6). The gene position within the network indicates how it overlaps with other Minutes. Genes occupying a more central position are present in more than one Minute network. Thus, our graph shows that the majority of genes present on the network are shared by more than one RP module, indicating that RP modules are complementary. Furthermore, the network analysis also indicated a high connectedness between different RP genes (i.e. distance between genes inside a cluster) suggesting a common activation pathway.

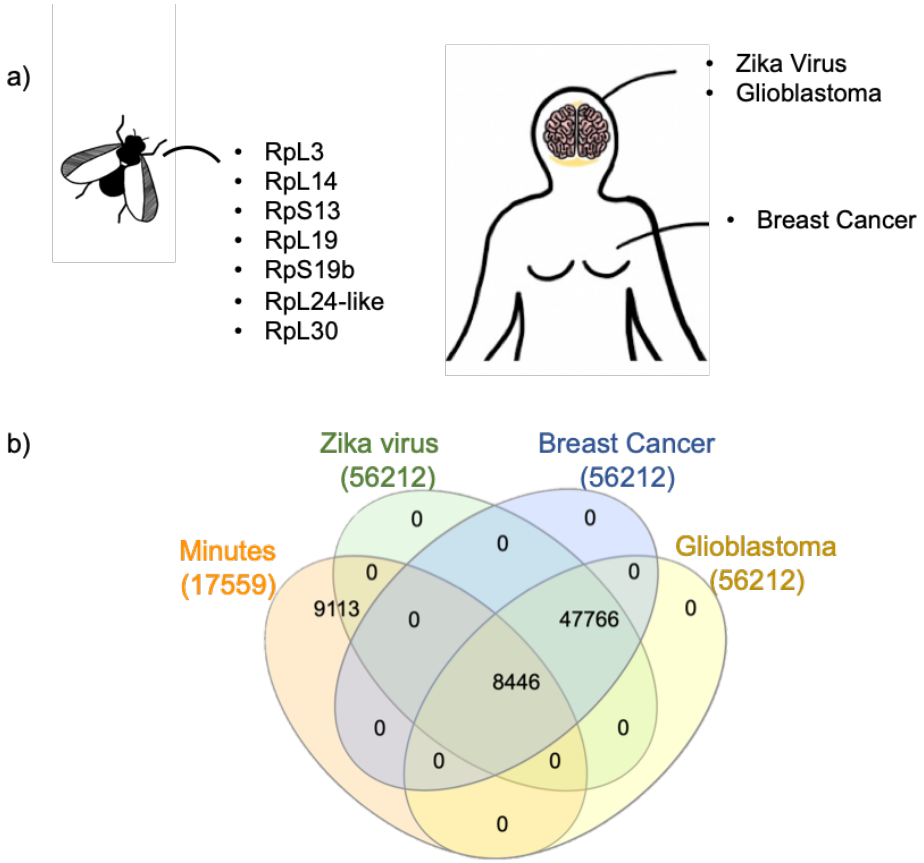

Figure 5 - Homologue comparison between fly and human datasets. a) Schematic representation of the WGCNA comparison between Minute mutants and glioblastoma, breast cancer and Zika virus infection transcriptome. b) Venn Diagram of shared genes between Minute mutants and glioblastoma, breast cancer and Zika virus infection.

Table 6 - Overview of module preservation statistics. Columns report RP modules compared and preservation statistics (ZSummary and p-value) for each set of data (Glioblastoma, breast cancer and Zika virus). A Zsummary statistic of >10 is considered strongly similar, >5 moderately similar and <2 as dissimilar.

	Glioblastoma vs RPs.		Breast Cancer vs RPs.		ZikaV vs RPs.	
	Zsummary	**p-value**	**Zsummary**	**p-value**	**Zsummary**	**p-value**
RpL3	9.561	<0.0001	7.678	<0.0001	0.094	0.710
RpL14	10.138	<0.0001	-4.550	0.977	-1.425	0.929
RpS13	7.287	<0.0001	5.892	0.0001	2.178	0.149
RpL19	-0.739	0.8961	-3.161	0.908	0.297	0.601
RpS19b	6.060	<0.0001	5.254	0.0002	1.847	0.216
RpL24-like	12.764	<0.0001	9.447	<0.0001	2.242	0.116
RpL30	8.088	<0.0001	4.281	0.0002	-0.821	0.838

Figure 6 - Cluster network of RP genes present in well-conserved modules in glioblastoma data. The co-expression network for each Rp group can be visualised as network components of genes that are exclusive or shared with other modules. Nodes are sized by intramolecular connectivity and coloured by Rp group or shared Rp network. Mutant genes are highlighted in red and labeled.

Discussion

Here we demonstrate that mutations affecting levels of RPs and causing the Minute phenotype result in highly pleiotropic gene-level transcriptomic changes. When viewed at the level of single-gene differential expression, these lack a clearly defined core of differentially expressed genes across the whole organism. Moreover, there is also no clear pattern or master regulator shaping the expression of RPs. Despite this pleiotropy, when network-based analysis is employed, a high degree of preservation between transcriptomes of all RP mutants was identified. Thus, what may appear stochastic or pleiotropic at one level, reveals a consistent pattern at a different level. This shaping of the entire RP mutant transcriptome bears striking similarity to the transcriptomes of cancer cells.

Genomic Clustering

We found no evidence of genomic clustering of RP-encoding genes. Gene families are often clustered into "neighborhoods" to facilitate co-regulation (Cera et al., 2019; Spellman and Rubin, 2002). However, this is not the case with *D. melanogaster* RPs, as they appear randomly distributed throughout the genome. Furthermore, previous work identified several RP-encoding genes in close proximity, but did not offer any evidence of co-regulation (Marygold et al., 2007). Co-regulation through genomic clustering is linked to the influence of regulatory elements, such as enhancers, and to chromosome structure. Although effects of these elements can be mitigated by insulating genomic regions, genetic distance may be the most straightforward way to ensure independent regulation. Genomic spacing of RPs potentially permits single-gene transcriptional regulation and greater degree of fine-tuning compensatory regulation.

Differential Gene Expression & Regulation

These seven RP mutations lack a clear core of differentially expressed genes, with only 18 being shared among the seven analysed mutants (Supplementary Table S1). Thus, despite tightly controlled regulation and a shared role in ribosome biogenesis, RP mutations alter expression of individual genes in vastly different ways.

Although lacking a core, there remains a high degree of overlap, either in pairwise or sub-group comparisons (Figure 2) between differentially expressed genes in these mutants. The largest overlap of differentially expressed transcripts (441) occurs between RpL24-like, RpS19b, RpL3, and RpL30 (Figure 2). This overlap does not relate to the size of the RP, nor to their position within an assembled ribosome (Anger et al., 2013). The overlap is likely because these mutants have the largest number of differentially expressed transcripts. This certainly does not rule out an underlying biological cause for high levels of differential expression and overlap, but it does reinforce the absence of a clearly defined core.

Finally, and further highlighting variability between their transcriptomes, each of these RPs mutants has a considerable number of uniquely differentially expressed genes (Table 2). These range from 9% of all differentially expressed genes in RpL30 to 28% in RpS13 with an average of 17% across all seven.

It is important to reiterate that our observations are based on four replicates of whole individual flies rather than on pooled samples of specific tissues. Therefore, we would not detect small tissue-specific or temporally-specific responses, but rather macro responses. Although cell- and timing-specific RP functions are critical, they are likely tightly regulated and impossible to generalise. We were unable to detect previously identified *D. melanogaster* RP regulators in either differential expression analysis 2 or Differential Network Analysis (Table 3). This is unsurprising as individual RPs can have highly specific extra-ribosomal functions (Warner and McIntosh, 2009) and are differentially assembled into ribosomes depending on functional or tissue-specific factors (Genuth and Barna, 2018). Rapidly dividing tissues, such as the imaginal disks, likely have elevated or specialised ribosome biogenesis, a conclusion that is supported by the elevated expression of RP encoding genes in this tissue (Brown et al., 2014; Celniker et al., 2009).

In addition, we also examined single-gene markers that have been previously identified as being misregulated in response to mutations affecting RPs (Supplementary Table S2). Once again, no clear core pathway can be identified. Only five genes, asp (cytoskeleton), CycB3 (cell cycle), pik92e (cell and tissue growth), ask1 (JNK pathway) & bsk (JNK pathway), of the twenty candidates examined, representing major cellular regulatory pathways, were misregulated in four or more of the RP mutations. This does not suggest that these cellular processes are not intricately linked to RPs. For example, it is well known that the Toll-apoptosis results in cell elimination of RP mutant cells, when in competition with wild type cells, (Meyer et al., 2014). However, this, like other regulatory or pathway examples, is likely highly context-specific; thus, it is potentially missed when examining RPs at the macro level.

Dosage Effects

Dosage changes in RP expression, regardless of direction, appear to have similar transcriptomic effects. The strongly overexpressed mutant *RpS19* resulted in the second highest number of differentially expressed genes (Table 2). Moreover, there was considerable overlap in differentially expressed genes of RpS19 with those of other RP mutants (Figure 2). Dose-dependency is critical in ribosome biogenesis, with overexpression of RPs being linked to disruption of this process (Tye et al., 2019). Moreover, overexpression of several RPs has been linked to cancer (discussed below).

As only one of the seven Minute mutants screened over-expressed the corresponding RP, it is possible that RP overexpression doesn't generally result in Minute phenotypes. Moreover, the large overexpression of *RpS19*, compared with underexpression seen with other RPs perhaps suggests that RPs are less sensitive to overexpression. Although this observation does highlight the delicate balance that RPs maintain, further conclusions are impossible without generating a series of strains with overexpressed RP encoding genes

Function & Network Analysis

The discovery of regulatory networks and pathways are an important step in understanding the mechanisms of complex diseases, and discovering biomarkers and drug targets. As demonstrated in our results, traditional differential gene expression analysis cannot fully grasp the complexity of RP-induced transcriptomic changes. Using

two different network analyses (WGCNA and DCE), we identified ribosomal pathways (modules) and how these pathways change in response to ribosomal protein mutations, indicating a large compensatory mechanism. Although both analyses yielded a similar result, we identified RP-hub genes associated with each mutant using WGCNA due to its powerful network estimation. We also showed that these RP modules are highly preserved across all RP mutants strains , as well as displaying a high connectedness (Figure 6). These results indicate the presence of an underlying co-regulation common to all mutants. It also provides strong evidence that RP hub genes are involved in the same biological pathways, as they have similar expression levels and preservation. GO term analysis failed to identify the same pattern, attributing different functions to our RP hub genes and contradicting the network analysis.

GO analysis, while useful, provides only a crude view of how the transcriptomic network is altered. As it relies on a list of differentially expressed genes, a conservative analysis can fail to identify key GO terms. Moreover, differentially expressed genes can fall into several GO biological process categories. Complex traits, such as disease or disruption of key biological processes can result in high numbers of genome-wide associations. In these instances, GO analysis typically correlates with the number of gene members in a specific GO category (Boyle et al., 2017). Therefore, the use of network analysis to group functionally related genes provides a more comprehensive reference framework for the understanding of regulation of ribosomal genes and the networks associated with them.

Given the importance of ribosomal biogenesis for cellular health, growth and homeostasis, it has been proposed that all ribosomal components are tightly co-regulated (Coléno-Costes et al., 2012; Reja et al., 2015; Li et al., 2018). The analysis employed here provides a novel demonstration of interrelated regulation of the RPs.

Cancer, Zika virus & Ribosomal Proteins

There are several excellent studies that highlight the contributions of RPs to oncogenesis when mutated, and their aberrant expression is often observed in cancerous cells (Bee et al., 2011; Henry et al., 1993; Hong et al., 2014; Lai et al., 2009; Oršolić et al., 2020). In this study, we used WGCNA to construct a co-expression network for identification of gene co-expression modules associated with glioblastoma and breast cancer. We identified 5 RP modules and over 4000 genes closely related to glioblastoma and 3 modules with over 5000 genes related to Breast cancer. Cancers have been widely reported to vary greatly at the transcriptomic level. In fact, different types of cancer arising from the same lineage exhibit tissue-specific gene over-expression (Axelsen et al., 2007). Given the enormous variation in cancer transcriptomics and the RPs analysed, it is reasonable that a target gene approach resulted in a large gene network associated with cancer development.

Disruption of RPs closely mimics transcriptional networks observed in cancers. As one might expect, genes strongly upregulated in several cancers, such as RpL19 (Henry et al., 1993; Hong et al., 2014), do not mimic cancer networks when mutated. Moreover, downregulation of RpL19 in a prostate cancer cell line reduced aberrant growth (Bee et al., 2011). Both differential gene expression and network expression analyses revealed cancer-like transcriptomic responses in RpL24-like and RpS3 mutants. Moreover, all of the Minute RP mutants had at least some cancer markers differentially expressed, or displayed cancer-like transcriptomic networks, especially in RpL24-like mutants.

However, we failed to identify a key common core between RP mutations and Zika virus responses. Flaviviruses, such as Zika virus, have a single-stranded RNA genome that serves as both a messenger for translation and a template for replication (Garcia-Blanco et al., 2016). To efficiently replicate, they depend on cellular translational machinery to produce viral proteins required for replication. As a result, they have evolved efficient mechanisms to modify or even inhibit host protein translation (Sanford et al., 2019). This alteration of host translational mechanisms, as opposed to disruption or overexpression of ribosomal genes, as occurs in RP mutations, could explain why we failed to identify a well-conserved gene core between them. Furthermore, a ModulePreservation comparison between glioblastoma and Zika virus-infected neuroblastoma cells identified a smaller set of preserved RP hub genes than Minutes and glioblastoma, indicating that glioblastoma has a co-expression pattern more similar to RP mutations in fruit flies than to neuroblastoma, further reinforcing the role of RP regulation in cell machinery.

The seven mutant RPs we examined lacked a cancer-like universal marker. Although some RPs misexpressed genetic cancer markers, this was not universal. Of the markers tested, no gene was aberrantly expressed in more than five of the seven RP mutant backgrounds (Table S2).

Our work highlights the potential for *D. melanogaster* Minute mutations to act, not only as models of RPs, but of numerous pathologies. Although there is no shortage of model systems for disease studies, the tools available to *Drosophila* specialists continue to ensure the relevance of this model organism. For example, this work highlights the potential of the Minute system for studying the functions that perturbations in ribosome biogenesis serve in human disease. Moreover, there may also be utility in the system for rapid screening of genes involved in oncogenesis.

Genome Stability

As RPs assemble in precise relationships into functional ribosomes, imbalances in RP abundance can signal genomic destabilization, which is often associated with cancer development (Penzo et al., 2019). Thus, RPs can have extra-ribosomal roles as sentinels of genome stability (Warner and McIntosh, 2009) and may induce cell cycle arrest and cell death. This suggests that for cells to survive and proliferate in Minute individuals, some regulatory checkpoints have to be overcome in a manner resembling that of precancerous cells.

As shown here, small changes in RP encoding of transcript abundance can have a strong ripple effect throughout the entire transcriptome. Due to their role as gatekeepers of genomic integrity, there is potential for RPs to contribute to hybrid incompatibility. Small differences in regulation of RP-encoding genes between allospecific parents may result in negative fitness outcomes or Minute-like phenotypes. In addition to functions of RPs in oncogenesis and genome integrity, further study of their roles in hybrid incompatibility or underdominance is warranted.

Conclusion

Although RPs have typically been studied strictly with respect to their roles in ribosome biogenesis, a wealth of research suggests that RPs regulate critical cellular processes. Thus, additional links to cancer are to be expected. In our work, and throughout the literature, RP mutants display non-overlapping pleiotropic phenotypes. Despite the shared Minute phenotype, transcriptomic responses of RP mutants examined

here vary greatly at the individual gene level. However, when stepping back and examining not just the trees but the whole forest, it becomes clear that disruption of RPs shapes the transcriptome in similar ways. Furthermore, RP mutations induce changes in *D. melanogaster* that despite the huge evolutionary distances involved, are very similar to those in human cancers.

Materials & Methods

Fly Husbandry & Generation of RP Lines

Flies were raised on standard Bloomington media at 24 °C under a 16h light / 8h dark cycle in 50 mL vials.

Several Minute mutants constructed in prior studies by *P*-element insertion mutagenesis were obtained from the Bloomington *Drosophila* Stock Centre (BDSC) and were backcrossed for eight generations to control white-eyed line. Minute males marked with mini-*white* *w*[-]/Y; P{m*w*}/balancer were crossed to *w*[1] females. mini-*white* female offspring were selected without the balancer and crossed to *w*[1] males. This brought the Minute disruption into a common *w*[1] maternal (mitochondrial and cytoplasmic) and paternal (Y-chromosome) genetic background. Four additional generations of crosses were made in the *w*[1] background before maintaining the stocks as heterozygotes by selecting for m*w*. m*w* flies were crossed to *w*[1] in the final generation before collecting female offspring for RNA extraction. *w*[+] controls (Canton-S) were also generated by crossing wildtype males to w[1] females, selecting *w*[+]/*w*[1] female offspring to cross to *w*[1] males, and backcrossing to w[1] for three additional generations.

During back-crossing of both RpS24 and RpL26 two shades of red segregated flies. This suggests that these strains may contain multiple p-element insertions, and given the low frequency of the second eye colour in subsequent crosses, these p-elements are likely tightly linked. Therefore, these two mutants were removed from the experiment.

Table 7 - *Drosophila melanogaster* Strains Used.

Strain	Mutation	BDSC	Reference
RpL3	*P{w[+mC]=EP}RpL3[G13893]*	30199	(Bellen et al., 2004)
RpL14	*P{w[+mC]=lacW}RpL14[1]*	2247	(Sæbøe-Larssen et al., 1997)
RpL19	*P{w[+mC]=lacW}RpL19[k03704]*	12209	(Spradling et al., 1999)
RpL24-like	*P{w[+mC]=EP}RpL24-like[G5422]*	30157	(Bellen et al., 2004)
RpL30	*P{w[+mC]=lacW}RpL30[k00308]*	10303	(Spradling et al., 1999)
RpS13	*P{w[+mC]=lacW}RpS13[1]*	2246	(Sæbøe-Larssen and Lambertsson, 1996)
RpS19b	*PBac{w[+mC]=IT.GAL4}RpS19b[0743-G4]*	63769	(Gohl et al., 2011)
RpS24	*P{w[+mC]=laxW}RpS24[SH2053]*	29511	(Bellen et al., 2004)
RpL26	*PBac{w[+mC]=IT.GAL4}RpL26[0639-G4]*	63728	(Gohl et al., 2011)
white	Doc{}w[1]	145	(Morgan, 1910)
wildtype	Canton-S-SNPisoX	6364	(Hoskins et al., 2001)

RNA Extraction & Library Preparation

Whole RNA was extracted using a Qiagen RNeasy Micro kit from individual 2-day-old virgin female flies. Biological replicates for each strain listed in Table 7 were performed in quadruplicate (with the exception of RpS24 and RpL26 which have been omitted). RNA quality was assessed using both a NanoDrop (Thermo Scientific), and subsequently a BioAnalyser (Agilent). RNA library construction and subsequent sequencing were performed by the Okinawa Institute of Science and Technology DNA Sequencing Centre – Onna, Okinawa. Libraries were prepared with a TruSeq RNA Library Prep Kit version 2 (Illumina RS-122) and sequenced on an Illumina HiSeq4000 in paired-end mode (PE150).

Gene Differential Expression Analysis

All statistical analysis and results can be viewed at https://github.com/marivelasque/Minute_project.git. RNA data were trimmed with Trimmomatic 0.38 (Bolger et al., 2014) and quality was assessed using FASTQC (Andrews, 2010). Transcript abundance was calculated with RSEM/bowtie2 (Langmead and Salzberg, 2012; Li and Dewey, 2011). Mapping and abundance calculations were performed against the *D. melanogaster* genome assembly BDGP6 (release 89). Differential expression analysis was performed using DESEQ2 (Love et al., 2014). Visualization relied on packages UpSetR (Conway et al., 2017), ggplot2 (Wickham, 2009, p. 2), igraph (Csardi and Nepusz, 2006), circlize (Gu, 2014) and chorddiag (Gu, 2014). Analysis was run and figures generated using R in the RStudio environment. A markdown file containing the analysis pipeline and generated figures is available on GitHub (updated prior to publication).

Data Filtering

For both the differential gene expression analysis, conducted with DESEQ2 and WGCNA analysis, genes differentially expressed between white and wildtype were removed. A total of 1332 genes were differentially expressed between the white and wildtype. Removal of these genes from the analysis serves as a conservative control for the presence of a functional/semi-functional copy of the *white* gene.

Network Analysis

To estimate Differential Network Expression, we used the dnapath R package. To control the network differences in white, we removed all genes significantly co-expressed between white and wildtype. We removed a total of 1750 genes that were differentially co-expressed in white. Differential Network Expression was estimated using pairwise comparisons.

We used the WGCNA R package to construct the co-expression network using gene counts obtained from RSEM. Prior to the analysis, we removed gene outliers using the "goodSamplesGenes" function and accessed overall sample clustering in the expression matrix using "hclust." We used the lowest threshold power that resulted in approximate scale-free topology to construct the gene co-expression network using "blockwiseModules." Then, we estimated the gene expression profile, module eigengene,

and the module-treatment relationship, calculating the correlation between the module eigengene and treatment group. Modules that were significantly associated with the treatment were used to generate a gene network plot with the R package, igraph. We merged all treatment groups, generating a gene network plot for all treatment groups (Figure 6). Individual plots (i.e., each treatment group) can be found in the Supplemental Material (Figures S1-6).

To determine whether RP mutant modules were conserved groups, we used a WGCNA integrated function (modulePreservation) to calculate module preservation statistics, applied using two network-based composite preservation statistics (Zsummary). Zsummary results and respective p-values were generated through permutation testing (500 permutation). A Zsummary statistic of >10 is viewed as being strongly similar, >5 moderately similar and <2 as having no similarity (Langfelder et al., 2011). The R script used in this study is available at https://github.com/marivelasque/Minute_project.git.

We examined preservation of network properties of the ribosomal hub genes from mutants and two types of cancer, glioblastoma (Bioproject PRJNA388704) and breast cancer (Bioproject PRJNA484546; Rao et al., 2019) and Zika virus (Bioproject PRJNA497590; Martín et al., 2018). Raw reads were downloaded from NCBI and mapping and abundance calculations were performed using the same pipeline used for Minute data against the Genome Reference Consortium Human Build 38.

To establish universal gene identifiers and to facilitate comparisons between human and Minute data, we re-annotated human gene identifiers with *Drosophila melanogaster* gene orthologs. Only identifiers that were common to both data sets (human and fruit flies) were retained. We used the same approach to construct the gene co-expression network as described above. Next, we compared preservation of RP modules between human and Minute data using modulePreservation statistics from WGCNA software.

Network plots were generated by building an adjacency matrix from the RP group and module. The adjacency matrix was then converted into an igraph object and merged by gene name.

Declarations

Acknowledgements

We thank Kevin R. Cook (Indiana University Bloomington) and Steven J. Marygold (University of Cambridge) for advice, suggestions, comments on the manuscript and discussion of Minutes. We thank Heather Flores and Jarek Bryk for comments on the manuscript. We thank Steve D. Aird for editing the manuscript. Stocks obtained from the Bloomington *Drosophila* Stock Center (NIH P40OD018537) were used in this study. The Okinawa Institute of Science & Technology Sequencing Centre performed the RNA library preparations and generated the sequencing data.

Funding

The experiments and analysis were funded by the University of Hawai'i at Mānoa, National Institutes of Health COBRE P20 GM125508 awarded to FAR, the Okinawa Institute of Science & Technology and JSPS KAKENHI Grants 19K06795 and 19K16205

awarded to JAD and MV respectively. JAD and MV were supported by the Okinawa Institute of Science & Technology Genomics & Regulatory Systems Unit.

Availability of Data & Materials

All code is available at and a markdown file showing all analysis will be available on GitHub prior to publication (https://github.com/marivelasque/Minute_project.git.). All raw sequencing data will be made available prior to publication under the BioProject PRJDB10781.

Author Contributions

FAR conceived the project. JAD and FAR conducted the experiments. JAD, MV and FAR analyzed the results and wrote the paper.

References

Abdulkina, L.R., Kobayashi, C., Lovell, J.T., Chastukhina, I.B., Aklilu, B.B., Agabekian, I.A., Suescún, A.V., Valeeva, L.R., Nyamsuren, C., Aglyamova, G.V., Sharipova, M.R., Shippen, D.E., Juenger, T.E., Shakirov, E.V., 2019. Components of the ribosome biogenesis pathway underlie establishment of telomere length set point in Arabidopsis*. Nat. Commun.* 10, 5479. https://doi.org/10.1038/s41467-019-13448-z

Amsterdam, A., Sadler, K.C., Lai, K., Farrington, S., Bronson, R.T., Lees, J.A., Hopkins, N., 2004. Many Ribosomal Protein Genes Are Cancer Genes in Zebrafish*. PLoS Biol.* 2. https://doi.org/10.1371/journal.pbio.0020139

Andrews, S., 2010. FastQC: a quality control tool for high throughput sequence data [WWW Document]. URL http://www.bioinformatics.babraham.ac.uk/projects/fastqc

Anger, A.M., Armache, J.-P., Berninghausen, O., Habeck, M., Subklewe, M., Wilson, D.N., Beckmann, R., 2013. Structures of the human and *Drosophila* 80S ribosome*. Nature* 497, 80–85. https://doi.org/10.1038/nature12104

Axelsen, J.B., Lotem, J., Sachs, L., Domany, E., 2007. Genes overexpressed in different human solid cancers exhibit different tissue-specific expression profiles*. Proc. Natl. Acad. Sci.* 104, 13122–13127. https://doi.org/10.1073/pnas.0705824104

Bee, A., Brewer, D., Beesley, C., Dodson, A., Forootan, S., Dickinson, T., Gerard, P., Lane, B., Yao, S., Cooper, C.S., Djamgoz, M.B.A., Gosden, C.M., Ke, Y., Foster, C.S., 2011. siRNA Knockdown of Ribosomal Protein Gene RPL19 Abrogates the Aggressive Phenotype of Human Prostate Cancer*. PLOS ONE* 6, e22672. https://doi.org/10.1371/journal.pone.0022672

Bellen, H.J., Levis, R.W., Liao, G., He, Y., Carlson, J.W., Tsang, G., Evans-Holm, M., Hiesinger, P.R., Schulze, K.L., Rubin, G.M., Hoskins, R.A., Spradling, A.C., 2004. The BDGP gene disruption project: single transposon insertions associated with 40% of *Drosophila* genes.. *Genetics* 167, 761. https://doi.org/10.1534/genetics.104.026427

Bhuva, D.D., Cursons, J., Smyth, G.K., Davis, M.J., 2019. Differential co-expression-based detection of conditional relationships in transcriptional data: comparative analysis and application to breast cancer*. Genome Biol.* 20, 236. https://doi.org/10.1186/s13059-019-1851-8

Blanco, J., Cooper, J.C., Baker, N.E., 2020. Roles of C/EBP class bZip proteins in the growth and cell competition of Rp ('Minute') mutants in *Drosophila. eLife* 9, e50535. https://doi.org/10.7554/eLife.50535

Bolger, A.M., Lohse, M., Usadel, B., 2014. Trimmomatic: a flexible trimmer for Illumina sequence data*. Bioinformatics* 30, 2114–2120. https://doi.org/10.1093/bioinformatics/btu170

Boria, I., Garelli, E., Gazda, H.T., Aspesi, A., Quarello, P., Pavesi, E., Ferrante, D., Meerpohl, J.J., Kartal, M., Da Costa, L., Proust, A., Leblanc, T., Simansour, M., Dahl, N., Fröjmark, A.-S., Pospisilova, D., Cmejla, R., Beggs, A.H., Sheen, M.R., Landowski, M., Buros, C.M., Clinton, C.M., Dobson, L.J., Vlachos, A., Atsidaftos, E., Lipton, J.M., Ellis, S.R., Ramenghi, U., Dianzani, I., 2010. The ribosomal basis of Diamond-Blackfan Anemia: mutation and database update*. Hum. Mutat.* 31, 1269–1279. https://doi.org/10.1002/humu.21383

Boyle, E.A., Li, Y.I., Pritchard, J.K., 2017. An Expanded View of Complex Traits: From

Polygenic to Omnigenic. *Cell* 169, 1177–1186. https://doi.org/10.1016/j.cell.2017.05.038
Bridges, C.B., Morgan, T.H., Washington, C.I. of, 1923. The third-chromosome group of mutant characters of Drosophila melanogaster,. Carnegie Institution of Washington, Washington. https://doi.org/10.5962/bhl.title.24013
Brown, J.B., Boley, N., Eisman, R., May, G.E., Stoiber, M.H., Duff, M.O., Booth, B.W., Wen, J., Park, S., Suzuki, A.M., Wan, K.H., Yu, C., Zhang, D., Carlson, J.W., Cherbas, L., Eads, B.D., Miller, D., Mockaitis, K., Roberts, J., Davis, C.A., Frise, E., Hammonds, A.S., Olson, S., Shenker, S., Sturgill, D., Samsonova, A.A., Weiszmann, R., Robinson, G., Hernandez, J., Andrews, J., Bickel, P.J., Carninci, P., Cherbas, P., Gingeras, T.R., Hoskins, R.A., Kaufman, T.C., Lai, E.C., Oliver, B., Perrimon, N., Graveley, B.R., Celniker, S.E., 2014. Diversity and dynamics of the *Drosophila* transcriptome. *Nature* 512, 393–399. https://doi.org/10.1038/nature12962
Bursać, S., Brdovčak, M.C., Pfannkuchen, M., Orsolić, I., Golomb, L., Zhu, Y., Katz, C., Daftuar, L., Grabušić, K., Vukelić, I., Filić, V., Oren, M., Prives, C., Volarević, S., 2012. Mutual protection of ribosomal proteins L5 and L11 from degradation is essential for p53 activation upon ribosomal biogenesis stress. *Proc. Natl. Acad. Sci.* 109, 20467–20472. https://doi.org/10.1073/pnas.1218535109
Celniker, S.E., Dillon, L.A.L., Gerstein, M.B., Gunsalus, K.C., Henikoff, S., Karpen, G.H., Kellis, M., Lai, E.C., Lieb, J.D., MacAlpine, D.M., Micklem, G., Piano, F., Snyder, M., Stein, L., White, K.P., Waterston, R.H., 2009. Unlocking the secrets of the genome. *Nature* 459, 927–930. https://doi.org/10.1038/459927a
Cera, A., Holganza, M.K., Hardan, A.A., Gamarra, I., Eldabagh, R.S., Deschaine, M., Elkamhawy, S., Sisso, E.M., Foley, J.J., Arnone, J.T., 2019. Functionally Related Genes Cluster into Genomic Regions That Coordinate Transcription at a Distance in *Saccharomyces cerevisiae. mSphere* 4. https://doi.org/10.1128/mSphere.00063-19
Conway, J.R., Lex, A., Gehlenborg, N., 2017. UpSetR: an R package for the visualization of intersecting sets and their properties. *Bioinformatics* 33, 2938–2940. https://doi.org/10.1093/bioinformatics/btx364
Crow, M., Lim, N., Ballouz, S., Pavlidis, P., Gillis, J., 2019. Predictability of human differential gene expression. *Proc. Natl. Acad. Sci.* 116, 6491–6500. https://doi.org/10.1073/pnas.1802973116
Csardi, G., Nepusz, T., 2006. The igraph software package for complex network research. *InterJournal Complex Syst.* 1695.
De Keersmaecker, K., Atak, Z.K., Li, N., Vicente, C., Patchett, S., Girardi, T., Gianfelici, V., Geerdens, E., Clappier, E., Porcu, M., Lahortiga, I., Lucà, R., Yan, J., Hulselmans, G., Vranckx, H., Vandepoel, R., Sweron, B., Jacobs, K., Mentens, N., Wlodarska, I., Cauwelier, B., Cloos, J., Soulier, J., Uyttebroeck, A., Bagni, C., Hassan, B.A., Vandenberghe, P., Johnson, A.W., Aerts, S., Cools, J., 2013. Exome sequencing identifies mutation in CNOT3 and ribosomal genes RPL5 and RPL10 in T-cell acute lymphoblastic leukemia. *Nat. Genet.* 45, 186–190. https://doi.org/10.1038/ng.2508
Dolezal, J.M., Dash, A.P., Prochownik, E.V., 2018. Diagnostic and prognostic implications of ribosomal protein transcript expression patterns in human cancers. *BMC Cancer* 18. https://doi.org/10.1186/s12885-018-4178-z
Dong, Z., Zhu, C., Zhan, Q., Jiang, W., 2017. The roles of RRP15 in nucleolar formation, ribosome biogenesis and checkpoint control in human cells. *Oncotarget* 8, 13240–13252. https://doi.org/10.18632/oncotarget.14658

Fancello, L., Kampen, K.R., Hofman, I.J.F., Verbeeck, J., Keersmaecker, K.D., 2017. The ribosomal protein gene RPL5 is a haploinsufficient tumor suppressor in multiple cancer types. *Oncotarget* 8, 14462–14478. https://doi.org/10.18632/oncotarget.14895

Garcia-Blanco, M.A., Vasudevan, S.G., Bradrick, S.S., Nicchitta, C., 2016. Flavivirus RNA transactions from viral entry to genome replication. *Antiviral Res.* 134, 244–249. https://doi.org/10.1016/j.antiviral.2016.09.010

Genuth, N.R., Barna, M., 2018. The discovery of ribosome heterogeneity and its implications for gene regulation and organismal life. *Mol. Cell* 71, 364–374. https://doi.org/10.1016/j.molcel.2018.07.018

Gohl, D.M., Silies, M.A., Gao, X.J., Bhalerao, S., Luongo, F.J., Lin, C.-C., Potter, C.J., Clandinin, T.R., 2011. A versatile in vivo system for directed dissection of gene expression patterns. *Nat. Methods* 8, 231–237. https://doi.org/10.1038/nmeth.1561

Henry, J.L., Coggin, D.L., King, C.R., 1993. High-Level Expression of the Ribosomal Protein L19 in Human Breast Tumors That Overexpress erbB-2. *Cancer Res.* 53, 1403–1408.

Hetman, M., Slomnicki, L.P., 2019. Ribosomal biogenesis as an emerging target of neurodevelopmental pathologies. *J. Neurochem.* 148, 325–347. https://doi.org/10.1111/jnc.14576

Hong, M., Kim, H., Kim, I., 2014. Ribosomal protein L19 overexpression activates the unfolded protein response and sensitizes MCF7 breast cancer cells to endoplasmic reticulum stress-induced cell death. *Biochem. Biophys. Res. Commun.* 450, 673–678. https://doi.org/10.1016/j.bbrc.2014.06.036

Hoskins, R.A., Phan, A.C., Naeemuddin, M., Mapa, F.A., Ruddy, D.A., Ryan, J.J., Young, L.M., Wells, T., Kopczynski, C., Ellis, M.C., 2001. Single Nucleotide Polymorphism Markers for Genetic Mapping in *Drosophila melanogaster. Genome Res.* 11, 1100–1113. https://doi.org/10.1101/gr.178001

Hsiao, T.-H., Chiu, Y.-C., Hsu, P.-Y., Lu, T.-P., Lai, L.-C., Tsai, M.-H., Huang, T.H.-M., Chuang, E.Y., Chen, Y., 2016. Differential network analysis reveals the genome-wide landscape of estrogen receptor modulation in hormonal cancers. *Sci. Rep.* 6, 23035. https://doi.org/10.1038/srep23035

Kim, D.-U., Hayles, J., Kim, D., Wood, V., Park, H.-O., Won, M., Yoo, H.-S., Duhig, T., Nam, M., Palmer, G., Han, S., Jeffery, L., Baek, S.-T., Lee, H., Shim, Y.S., Lee, M., Kim, L., Heo, K.-S., Noh, E.J., Lee, A.-R., Jang, Y.-J., Chung, K.-S., Choi, S.-J., Park, J.-Y., Park, Y., Kim, H.M., Park, S.-K., Park, H.-J., Kang, E.-J., Kim, H.B., Kang, H.-S., Park, H.-M., Kim, K., Song, K., Song, K.B., Nurse, P., Hoe, K.-L., 2010. Analysis of a genome-wide set of gene deletions in the fission yeast *Schizosaccharomyces pombe. Nat. Biotechnol.* 28, 617–623. https://doi.org/10.1038/nbt.1628

Kongsuwan, K., Yu, Q., Vincent, A., Frisardi, M.C., Rosbash, M., Lengyel, J.A., Merriam, J., 1985. A *Drosophila* Minute gene encodes a ribosomal protein. *Nature* 317, 555–558. https://doi.org/10.1038/317555a0

Kucinski, I., Dinan, M., Kolahgar, G., Piddini, E., 2017. Chronic activation of JNK JAK/STAT and oxidative stress signalling causes the loser cell status. *Nat. Commun.* 8, 136. https://doi.org/10.1038/s41467-017-00145-y

Lai, K., Amsterdam, A., Farrington, S., Bronson, R.T., Hopkins, N., Lees, J.A., 2009. Many ribosomal protein mutations are associated with growth impairment and tumor predisposition in zebrafish. *Dev. Dyn.* 238, 76–85. https://doi.org/10.1002/dvdy.21815

Lambertsson, A., 1998. 3 The Minute Genes in *Drosophila* and Their Molecular

Functions*, in: Hall, J.C., Dunlap, J.C., Friedmann, T., Giannelli, F. (Eds.), Advances in Genetics*. Academic Press, pp. 69–134. https://doi.org/10.1016/S0065-2660(08)60142-X
Langfelder, P., Horvath, S., 2008. WGCNA: an R package for weighted correlation network analysis*. BMC Bioinformatics* 9, 559. https://doi.org/10.1186/1471-2105-9-559
Langfelder, P., Luo, R., Oldham, M.C., Horvath, S., 2011. Is My Network Module Preserved and Reproducible?. *PLOS Comput. Biol.* 7, e1001057. https://doi.org/10.1371/journal.pcbi.1001057
Langmead, B., Salzberg, S.L., 2012. Fast gapped-read alignment with Bowtie 2*. Nat. Methods* 9, 357–359. https://doi.org/10.1038/nmeth.1923
Lee, C.-H., Kiparaki, M., Blanco, J., Folgado, V., Ji, Z., Kumar, A., Rimesso, G., Baker, N.E., 2018. A Regulatory Response to Ribosomal Protein Mutations Controls Translation, Growth, and Cell Competition*. Dev. Cell* 46, 456-469.e4. https://doi.org/10.1016/j.devcel.2018.07.003
Li, B., Dewey, C.N., 2011. RSEM: accurate transcript quantification from RNA-Seq data with or without a reference genome*. BMC Bioinformatics* 12, 323. https://doi.org/10.1186/1471-2105-12-323
Marygold, S.J., Roote, J., Reuter, G., Lambertsson, A., Ashburner, M., Millburn, G.H., Harrison, P.M., Yu, Z., Kenmochi, N., Kaufman, T.C., Leevers, S.J., Cook, K.R., 2007. The ribosomal protein genes and Minute loci of *Drosophila melanogaster. Genome Biol.* 8, R216. https://doi.org/10.1186/gb-2007-8-10-r216
McGowan, K.A., Li, J.Z., Park, C.Y., Beaudry, V., Tabor, H.K., Sabnis, A.J., Zhang, W., Fuchs, H., de Angelis, M.H., Myers, R.M., Attardi, L.D., Barsh, G.S., 2008. Ribosomal mutations cause p53-mediated dark skin and pleiotropic effects*. Nat. Genet.* 40, 963–970. https://doi.org/10.1038/ng.188
Meyer, S.N., Amoyel, M., Bergantiños, C., Cova, C. de la, Schertel, C., Basler, K., Johnston, L.A., 2014. An ancient defense system eliminates unfit cells from developing tissues during cell competition*. Science* 346. https://doi.org/10.1126/science.1258236
Moin, M., Bakshi, A., Saha, A., Dutta, M., Madhav, S.M., Kirti, P.B., 2016. Rice Ribosomal Protein Large Subunit Genes and Their Spatio-temporal and Stress Regulation*. Front. Plant Sci.* 7. https://doi.org/10.3389/fpls.2016.01284
Morgan, T.H., 1910. Sex Limited Inheritance in Drosophila*. Science* 32, 120–122. https://doi.org/10.1126/science.32.812.120
Nicolas, E., Parisot, P., Pinto-Monteiro, C., de Walque, R., De Vleeschouwer, C., Lafontaine, D.L.J., 2016. Involvement of human ribosomal proteins in nucleolar structure and p53-dependent nucleolar stress*. Nat. Commun.* 7, 11390. https://doi.org/10.1038/ncomms11390
Oršolić, I., Bursać, S., Jurada, D., Drmić Hofman, I., Dembić, Z., Bartek, J., Mihalek, I., Volarević, S., 2020. Cancer-associated mutations in the ribosomal protein L5 gene dysregulate the HDM2/p53-mediated ribosome biogenesis checkpoint*. Oncogene* 39, 3443–3457. https://doi.org/10.1038/s41388-020-1231-6
Penzo, M., Montanaro, L., Treré, D., Derenzini, M., 2019. The Ribosome Biogenesis—Cancer Connection*. Cells* 8. https://doi.org/10.3390/cells8010055
Pestov, D.G., Strezoska, Z., Lau, L.F., 2001. Evidence of p53-dependent cross-talk between ribosome biogenesis and the cell cycle: effects of nucleolar protein Bop1 on G(1)/S transition*. Mol. Cell. Biol.* 21, 4246–4255. https://doi.org/10.1128/MCB.21.13.4246-4255.2001

Rao, S., Lee, S.-Y., Gutierrez, A., Perrigoue, J., Thapa, R.J., Tu, Z., Jeffers, J.R., Rhodes, M., Anderson, S., Oravecz, T., Hunger, S.P., Timakhov, R.A., Zhang, R., Balachandran, S., Zambetti, G.P., Testa, J.R., Look, A.T., Wiest, D.L., 2012. Inactivation of ribosomal protein L22 promotes transformation by induction of the stemness factor, Lin28B. *Blood* 120, 3764–3773. https://doi.org/10.1182/blood-2012-03-415349

Sæbøe-Larssen, S., Lambertsson, A., 1996. A Novel *Drosophila* Minute Locus Encodes Ribosomal Protein S13. *Genetics* 143, 877–885.

Sæbøe-Larssen, S., Mohebi, B.U., Lambertsson, A., 1997. The *Drosophila* ribosomal protein L14-encoding gene, identified by a novel Minute mutation in a dense cluster of previously undescribed genes in cytogenetic region 66D. *Mol. Gen. Genet. MGG* 255, 141–151. https://doi.org/10.1007/s004380050482

Sanford, T.J., Mears, H.V., Fajardo, T., Locker, N., Sweeney, T.R., 2019. Circularization of flavivirus genomic RNA inhibits de novo translation initiation. *Nucleic Acids Res.* 47, 9789–9802. https://doi.org/10.1093/nar/gkz686

Slomnicki, L.P., Chung, D.-H., Parker, A., Hermann, T., Boyd, N.L., Hetman, M., 2017. Ribosomal stress and Tp53-mediated neuronal apoptosis in response to capsid protein of the Zika virus. *Sci. Rep.* 7, 16652. https://doi.org/10.1038/s41598-017-16952-8

Song, Y., Mugavero, J., Stauft, C.B., Wimmer, E., 2019. Dengue and Zika Virus 5′ Untranslated Regions Harbor Internal Ribosomal Entry Site Functions. *mBio* 10. https://doi.org/10.1128/mBio.00459-19

Spellman, P.T., Rubin, G.M., 2002. Evidence for large domains of similarly expressed genes in the *Drosophila* genome. *J. Biol.* 1, 5.

Spradling, A.C., Stern, D., Beaton, A., Rhem, E.J., Laverty, T., Mozden, N., Misra, S., Rubin, G.M., 1999. The Berkeley Drosophila Genome Project gene disruption project: Single P-element insertions mutating 25% of vital *Drosophila* genes. *Genetics* 153, 135–177.

Tye, B.W., Commins, N., Ryazanova, L.V., Wühr, M., Springer, M., Pincus, D., Churchman, L.S., 2019. Proteotoxicity from aberrant ribosome biogenesis compromises cell fitness. *eLife* 8, e43002. https://doi.org/10.7554/eLife.43002

Volarević, S., Stewart, M.J., Ledermann, B., Zilberman, F., Terracciano, L., Montini, E., Grompe, M., Kozma, S.C., Thomas, G., 2000. Proliferation, But Not Growth, Blocked by Conditional Deletion of 40S Ribosomal Protein S6. *Science* 288, 2045–2047. https://doi.org/10.1126/science.288.5473.2045

Wang, W., Nag, S., Zhang, X., Wang, M.-H., Wang, H., Zhou, J., Zhang, R., 2015. Ribosomal Proteins and Human Diseases: Pathogenesis, Molecular Mechanisms, and Therapeutic Implications. *Med. Res. Rev.* 35, 225–285. https://doi.org/10.1002/med.21327

Warner, J.R., McIntosh, K.B., 2009. How Common are Extra-ribosomal Functions of Ribosomal Proteins?. *Mol. Cell* 34, 3–11. https://doi.org/10.1016/j.molcel.2009.03.006

Weijers, D., Franke-van Dijk, M., Vencken, R.J., Quint, A., Hooykaas, P., Offringa, R., 2001. An *Arabidopsis* Minute-like phenotype caused by a semi-dominant mutation in a RIBOSOMAL PROTEIN S5 gene. *Dev. Camb. Engl.* 128, 4289–4299.

Weirauch, M.T., 2011. Gene Coexpression Networks for the Analysis of DNA Microarray Data, *in: Applied Statistics for Network Biology*. John Wiley & Sons, Ltd, pp. 215–250. https://doi.org/10.1002/9783527638079.ch11

Wickham, H., 2009. ggplot2: Elegant Graphics for Data Analysis, *Use R!*. Springer-Verlag,

New York. https://doi.org/10.1007/978-0-387-98141-3
Wolfe, C.J., Kohane, I.S., Butte, A.J., 2005. Systematic survey reveals general applicability of "guilt-by-association" within gene coexpression networks. *BMC Bioinformatics* 6, 227. https://doi.org/10.1186/1471-2105-6-227
Yassin, A., Fredrick, K., Mankin, A.S., 2005. Deleterious mutations in small subunit ribosomal RNA identify functional sites and potential targets for antibiotics. *Proc. Natl. Acad. Sci. U. S. A.* 102, 16620–16625. https://doi.org/10.1073/pnas.0508444102
Zheng, M., Wang, Yihua, Liu, X., Sun, J., Wang, Yunlong, Xu, Y., Lv, J., Long, W., Zhu, X., Guo, X., Jiang, L., Wang, C., Wan, J., 2016. The RICE MINUTE-LIKE1 (RML1) gene, encoding a ribosomal large subunit protein L3B, regulates leaf morphology and plant architecture in rice. *J. Exp. Bot.* 67, 3457–3469. https://doi.org/10.1093/jxb/erw167

Supplementary Figures

Table S1 - Core Genes. Gene names and IDs for differentially expressed genes (adj-p <0.05) that are common to all seven RP mutant lines. No filtering was performed for the direction of differential expression change.

Gene	Gene ID
Arr2	*FBgn0000121*
cni	*FBgn0000339*
CRMP	*FBgn0023023*
CG3740	*FBgn0023530*
CG14476	*FBgn0027588*
CG2930	*FBgn0028491*
CG1561	*FBgn0030317*
CG5613	*FBgn0030839*
CG8560	*FBgn0035781*
BoYb	*FBgn0037205*
CG2943	*FBgn0037530*
mask	*FBgn0043884*
CG31077	*FBgn0051077*
Atox1	*FBgn0052446*
Muc14A	*FBgn0052580*
Ctr1B	*FBgn0062412*
AGO2	*FBgn0087035*
CR43961	*FBgn0264676*

Table S2 - Differential Expression of Candidate Genes.

		RpS13		RpL24-like		RpL3		RpL30		RpS19b		RpL14		RpL19	
Gene	Homologue	Fold	adj-p	Fold	adj-p	Fold	adj-p	Fold	adj-p	Fold	adj-p	Fold	adj-p	Fold	adj-p
asp	**AspM**	**-0.1504**	**0.8470**	**1.2202**	**0.0002**	**0.9330**	**0.0081**	**0.9278**	**0.0094**	**0.9209**	**0.0071**	**0.4790**	**0.2276**	**0.4804**	**0.2411**
atk1	Akt1	-0.0150	0.9586	0.2965	0.0021	0.1881	0.0763	0.1551	0.1473	0.1095	0.3036	0.1034	0.3848	0.1103	0.3830
CG43333	POSTN	-0.5254	0.9164	-0.1925	0.9433	-0.7088	0.7828	-0.3615	0.8914	0.6903	0.7715	0.6470	0.8094	0.3725	0.9120
cycB3	**CCNB3**	**-0.3074**	**0.6850**	**1.1579**	**0.0024**	**0.9287**	**0.0244**	**0.8292**	**0.0458**	**0.9667**	**0.0145**	**0.5111**	**0.2666**	**0.4761**	**0.3332**
l(2)dtl	dtl	-0.2594	0.7087	0.8234	0.0190	0.5714	0.1385	0.5092	0.1870	0.7312	0.0419	0.5093	0.2214	0.1226	0.8277
eif2a	EIF2S1	0.1058	0.5483	0.0892	0.4066	0.1608	0.1309	0.0311	0.8042	0.0253	0.8333	0.0339	0.7972	-0.0341	0.8269
eif3a	EIF3A	0.1255	0.4407	0.3605	0.0002	0.3490	0.0005	0.1830	0.0798	0.1232	0.2359	0.0865	0.4662	0.0126	0.9407
foxo	Foxo1	0.3473	0.0339	0.1050	0.4788	-0.0229	0.8980	0.0362	0.8327	-0.0262	0.8750	0.0829	0.6226	0.4140	0.0034
fzy	Cdc20	-0.4370	0.5866	1.0642	0.0143	0.9069	0.0531	0.7416	0.1168	0.7381	0.1029	0.1963	0.7304	0.3594	0.5467
mps1	Ttk	-0.2641	0.6652	0.9196	0.0029	0.6619	0.0493	0.5733	0.0907	0.7607	0.0174	0.4021	0.2819	0.2491	0.5651
p53	Tp53	-0.5284	0.0103	-0.2466	0.1649	-0.3954	0.0290	-0.1403	0.4768	-0.1465	0.4354	-0.1305	0.5348	-0.0940	0.7028
pi3k92e	**Pik3CD**	**0.1486**	**0.4622**	**0.4334**	**0.0002**	**0.2958**	**0.0187**	**0.3230**	**0.0108**	**0.2202**	**0.0722**	**0.1508**	**0.2866**	**0.3325**	**0.0101**
sulf1	Sulf1	0.2873	0.0672	0.0887	0.5221	-0.0502	0.7473	0.1128	0.4201	0.0017	0.9919	0.2252	0.1149	0.4367	0.0006
tis11	Zfp36L2	0.1937	0.2102	0.1713	0.1230	0.1028	0.4125	0.1683	0.1505	0.0877	0.4653	0.0552	0.6941	0.2051	0.1001
top2	Top2A	0.1603	0.4921	0.2820	0.0365	-0.0631	0.7108	0.1424	0.3484	0.3547	0.0094	0.2084	0.1869	0.1131	0.5349
tor	mtor	0.0550	0.7050	0.3167	0.0000	0.0537	0.5453	0.1321	0.0950	0.1348	0.0738	0.0517	0.5762	0.1124	0.2052
ask1	**MAP3K15**	**0.0689**	**0.7248**	**0.5082**	**0.0000**	**0.4247**	**0.0000**	**0.3624**	**0.0003**	**0.2655**	**0.0069**	**0.1137**	**0.3266**	**0.2324**	**0.0304**
fmt	PPP6R2	0.2381	0.0195	0.3223	0.0001	0.1341	0.1447	0.1836	0.0407	0.1589	0.0651	0.0875	0.3895	0.2482	0.0060
tollo	tlr3	-0.2297	0.5996	-0.5341	0.0233	-0.6161	0.0130	0.0686	0.8208	-0.1374	0.6124	0.0944	0.7602	0.2389	0.4345
bsk	**MPK10**	**-0.0696**	**0.8335**	**-0.3520**	**0.0150**	**-0.3947**	**0.0097**	**-0.4094**	**0.0083**	**-0.3904**	**0.0086**	**-0.3120**	**0.0689**	**-0.3265**	**0.0465**

Table S3 - Shared Gene Ontology Categories of RP Mutants.

GO.ID	Term
GO:0043603	cellular amide metabolic process
GO:0034660	ncRNA metabolic process
GO:0006518	peptide metabolic process
GO:0043604	amide biosynthetic process
GO:0051234	establishment of localization
GO:0006399	tRNA metabolic process
GO:0043043	peptide biosynthetic process
GO:0008380	RNA splicing
GO:0006810	transport
GO:0000375	RNA splicing, via transesterification reactions
GO:0000377	RNA splicing, via transesterification reactions with bulged adenosine as nucleophile
GO:0000398	mRNA splicing, via spliceosome
GO:0034470	ncRNA processing
GO:0016192	vesicle-mediated transport
GO:0006412	translation
GO:0048646	anatomical structure formation involved in morphogenesis
GO:0009605	response to external stimulus
GO:0022613	ribonucleoprotein complex biogenesis
GO:1901564	organonitrogen compound metabolic process
GO:0009451	RNA modification
GO:0008033	tRNA processing
GO:0090066	regulation of anatomical structure size
GO:0071705	nitrogen compound transport

GO:0032940	secretion by cell
GO:0010941	regulation of cell death
GO:0043067	regulation of programmed cell death
GO:0070887	cellular response to chemical stimulus
GO:0042981	regulation of apoptotic process
GO:0046903	secretion
GO:0048193	Golgi vesicle transport
GO:0006629	lipid metabolic process
GO:0044255	cellular lipid metabolic process
GO:0002164	larval development
GO:0060541	respiratory system development
GO:0035151	regulation of tube size, open tracheal system
GO:0006400	tRNA modification
GO:0016310	phosphorylation
GO:0140053	mitochondrial gene expression
GO:0035150	regulation of tube size
GO:0071702	organic substance transport
GO:0006793	phosphorus metabolic process
GO:0008610	lipid biosynthetic process
GO:0023061	signal release
GO:0009062	fatty acid catabolic process
GO:0006796	phosphate-containing compound metabolic process
GO:0035152	regulation of tube architecture, open tracheal system
GO:0043038	amino acid activation
GO:0009056	catabolic process
GO:0043039	tRNA aminoacylation

GO:0016054	organic acid catabolic process
GO:0046395	carboxylic acid catabolic process
GO:0044281	small molecule metabolic process
GO:0016050	vesicle organization
GO:0006790	sulfur compound metabolic process
GO:0042592	homeostatic process
GO:0006418	tRNA aminoacylation for protein translation
GO:0072329	monocarboxylic acid catabolic process
GO:0034440	lipid oxidation
GO:0032543	mitochondrial translation
GO:0051186	cofactor metabolic process
GO:0006082	organic acid metabolic process
GO:0019395	fatty acid oxidation
GO:0006631	fatty acid metabolic process
GO:0044242	cellular lipid catabolic process
GO:0043436	oxoacid metabolic process
GO:0035159	regulation of tube length, open tracheal system
GO:0006414	translational elongation
GO:0120192	tight junction assembly
GO:0120193	tight junction organization
GO:0006635	fatty acid beta-oxidation
GO:1901137	carbohydrate derivative biosynthetic process
GO:0019752	carboxylic acid metabolic process
GO:0019991	septate junction assembly
GO:0006888	ER to Golgi vesicle-mediated transport
GO:0002181	cytoplasmic translation

GO:0002684	positive regulation of immune system process
GO:0031349	positive regulation of defense response
GO:0034330	cell junction organization
GO:0071826	ribonucleoprotein complex subunit organization
GO:0055114	oxidation-reduction process
GO:0022618	ribonucleoprotein complex assembly
GO:0048878	chemical homeostasis
GO:0006732	coenzyme metabolic process
GO:0045216	cell-cell junction organization
GO:0045087	innate immune response
GO:0033865	nucleoside bisphosphate metabolic process
GO:0033875	ribonucleoside bisphosphate metabolic process
GO:0034032	purine nucleoside bisphosphate metabolic process
GO:0032787	monocarboxylic acid metabolic process
GO:0044283	small molecule biosynthetic process
GO:0043297	apical junction assembly
GO:0007517	muscle organ development
GO:0007043	cell-cell junction assembly
GO:0050954	sensory perception of mechanical stimulus
GO:0016042	lipid catabolic process
GO:0019637	organophosphate metabolic process
GO:0045089	positive regulation of innate immune response
GO:0034329	cell junction assembly
GO:0072521	purine-containing compound metabolic process
GO:0009259	ribonucleotide metabolic process
GO:0051188	cofactor biosynthetic process

GO:0030198	extracellular matrix organization
GO:1901361	organic cyclic compound catabolic process
GO:0055086	nucleobase-containing small molecule metabolic process
GO:0030258	lipid modification
GO:0044282	small molecule catabolic process
GO:0042440	pigment metabolic process
GO:0006890	retrograde vesicle-mediated transport, Golgi to ER
GO:0009150	purine ribonucleotide metabolic process
GO:2000765	regulation of cytoplasmic translation
GO:1901615	organic hydroxy compound metabolic process
GO:0006897	endocytosis
GO:0006163	purine nucleotide metabolic process
GO:0019693	ribose phosphate metabolic process
GO:0009108	coenzyme biosynthetic process
GO:1901135	carbohydrate derivative metabolic process
GO:0090407	organophosphate biosynthetic process
GO:0006753	nucleoside phosphate metabolic process
GO:0009117	nucleotide metabolic process
GO:0046148	pigment biosynthetic process
GO:0055088	lipid homeostasis
GO:0007605	sensory perception of sound
GO:0046486	glycerolipid metabolic process
GO:0010876	lipid localization
GO:0006979	response to oxidative stress
GO:0016226	iron-sulfur cluster assembly
GO:0031163	metallo-sulfur cluster assembly

GO:0008202	steroid metabolic process
GO:0016053	organic acid biosynthetic process
GO:0046394	carboxylic acid biosynthetic process
GO:0006638	neutral lipid metabolic process
GO:0006639	acylglycerol metabolic process
GO:0016125	sterol metabolic process
GO:0006641	triglyceride metabolic process
GO:0006694	steroid biosynthetic process
GO:0035148	tube formation
GO:0042180	cellular ketone metabolic process
GO:0006644	phospholipid metabolic process

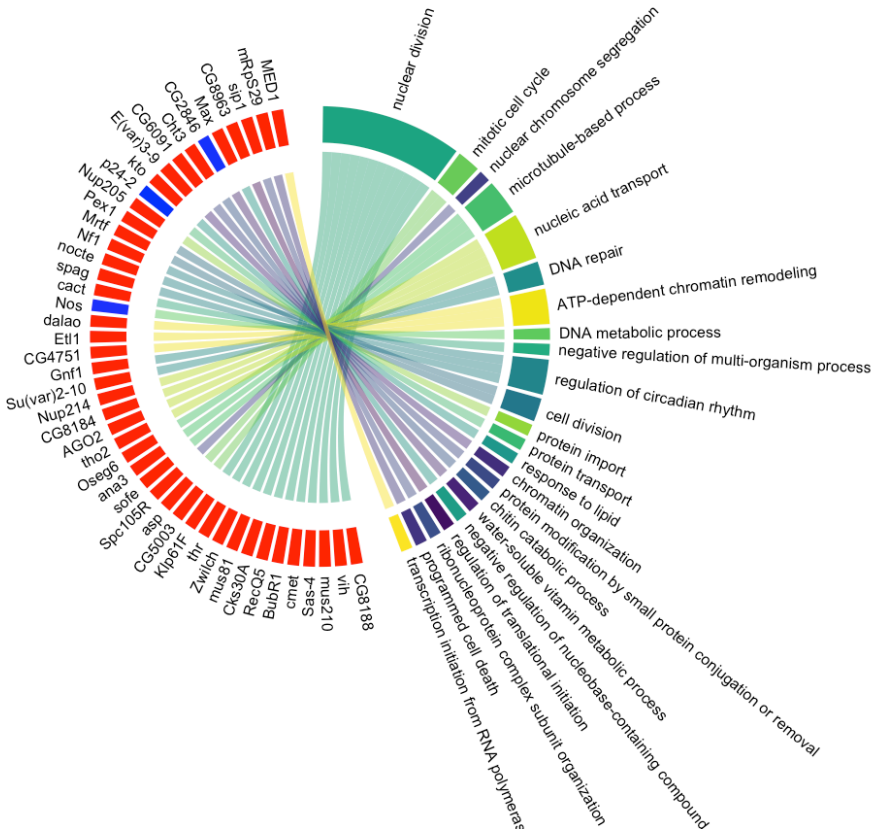

Figure S1. Circle plot of RpL3 mutants indicating the association between differentially expressed genes inside the "RpL3" gene cluster and their associated GO terms. Associations between individual genes and their terms are indicated with ribbons**.** Genes upregulated in the RpL3 module are represented in red and those downregulated in blue.

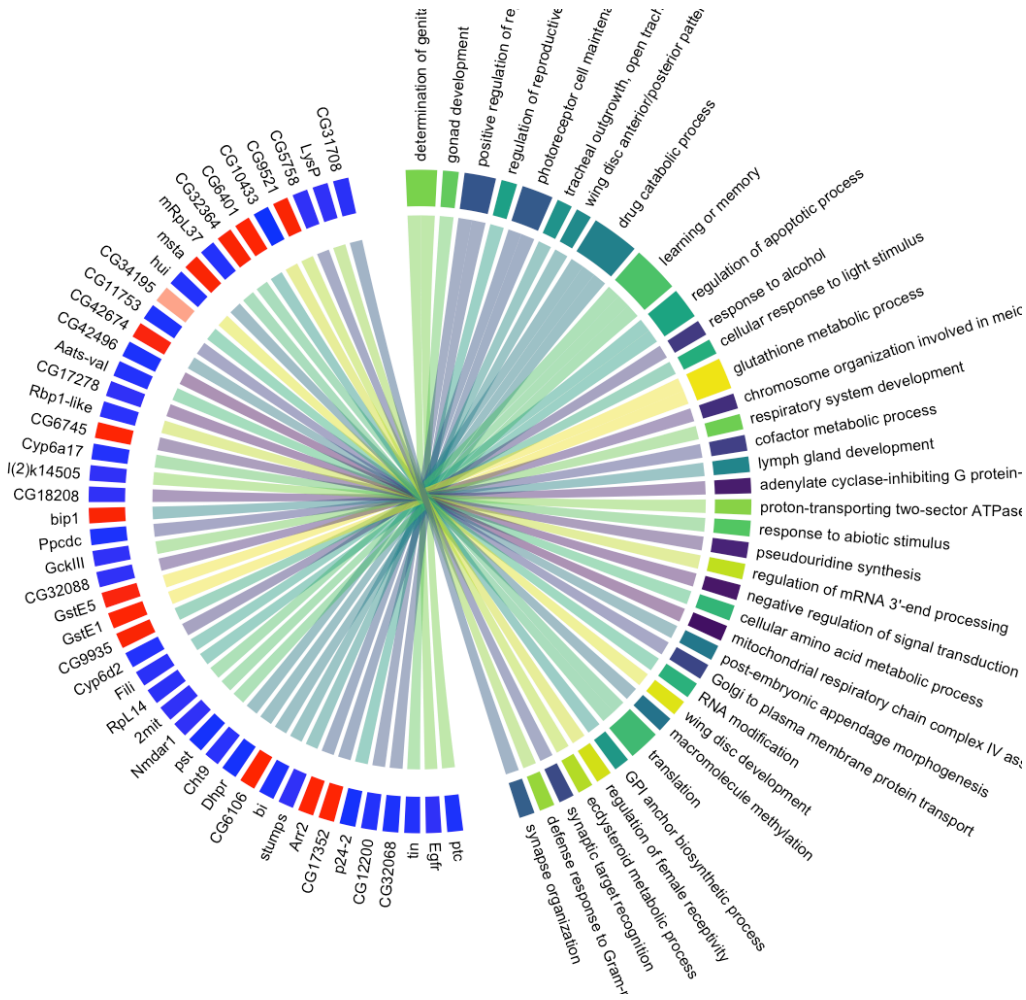

Figure S2. Circle plot of RpL14 mutants indicating the association between differentially expressed genes inside the "RpL14" gene cluster and their associated GO terms. Associations between individual genes and their terms are indicated with ribbons. Genes upregulated in the RpL14 module are represented in red and those downregulated in blue.

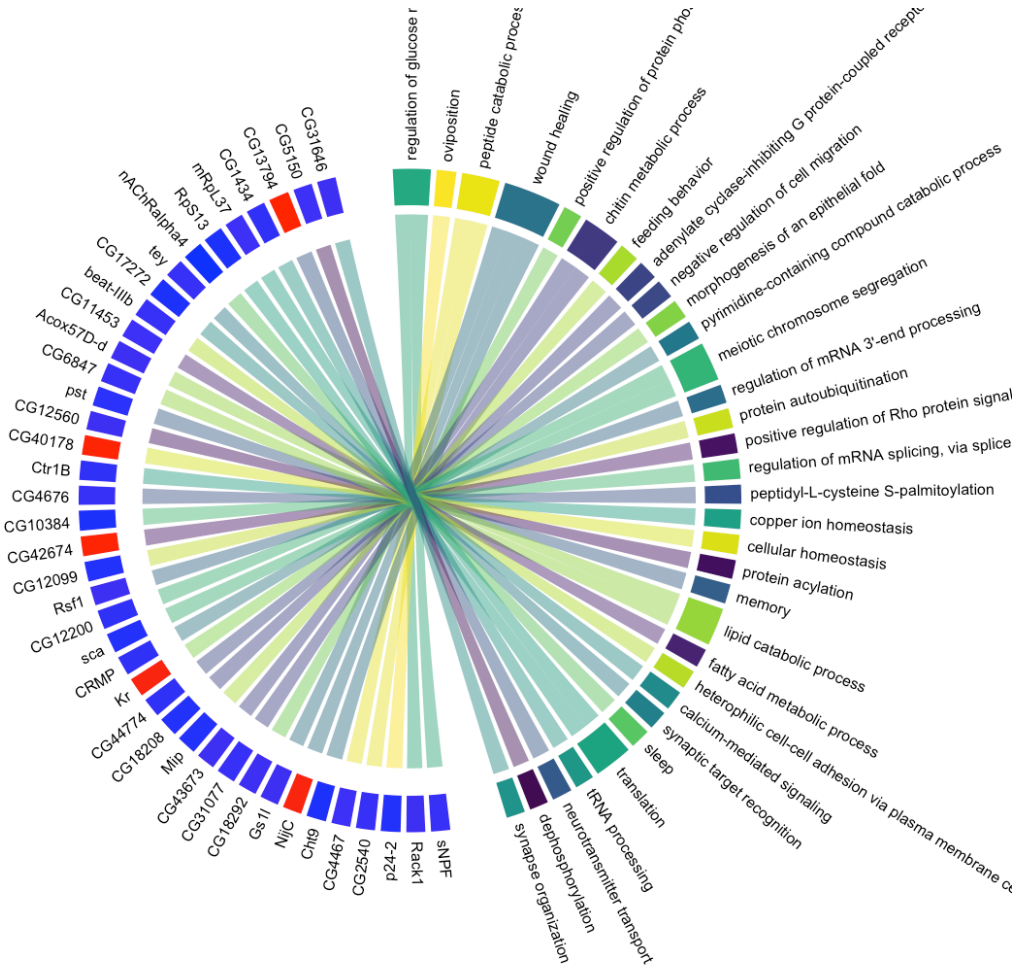

Figure S3. Circle plot of RpS13 mutants indicating the association between differentially expressed genes inside the "RpS13" gene cluster and their associated GO terms. Associations between individual genes and their terms are indicated with ribbons. Genes upregulated in the RpS13 module are represented in red and those downregulated in blue.

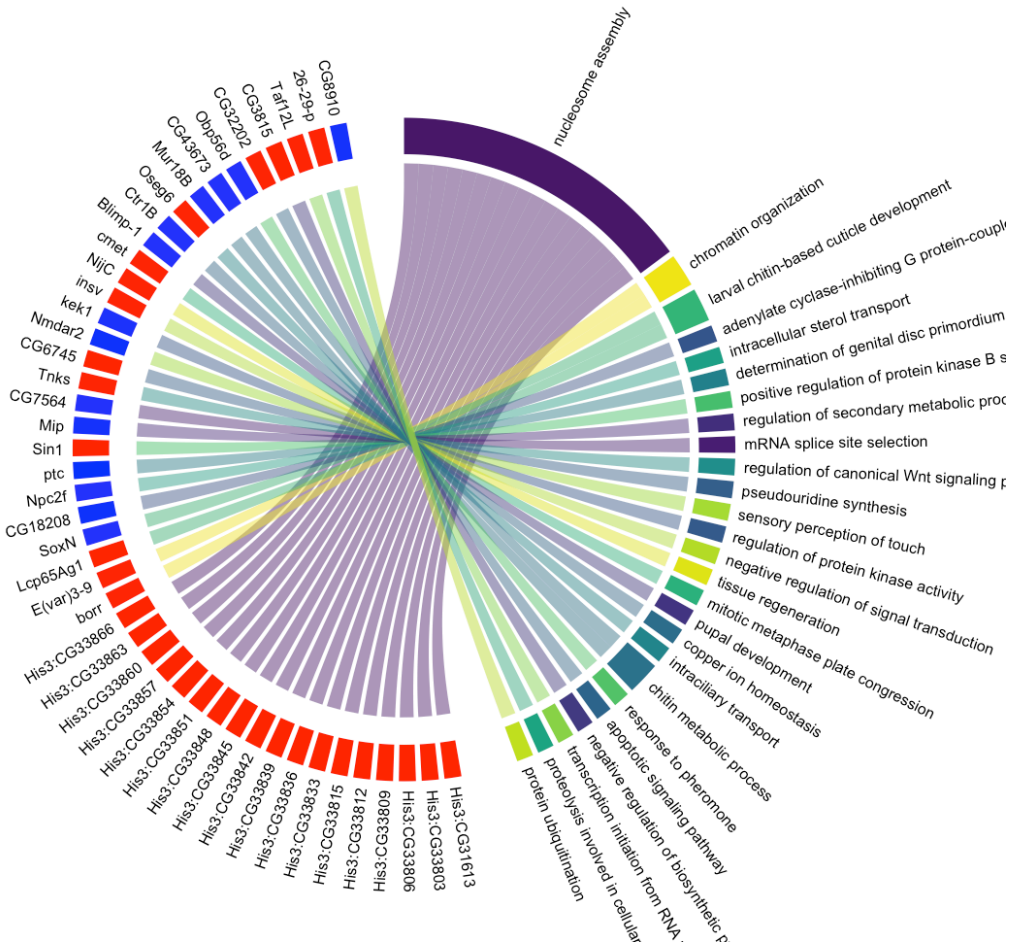

Figure S4. Circle plot of RpS19b mutants indicating the association between differentially expressed genes inside the "RpS19b" gene cluster and their associated GO terms. Associations between individual genes and their terms are indicated with ribbons. Genes upregulated in the RpS19b module are represented in red and those downregulated in blue.

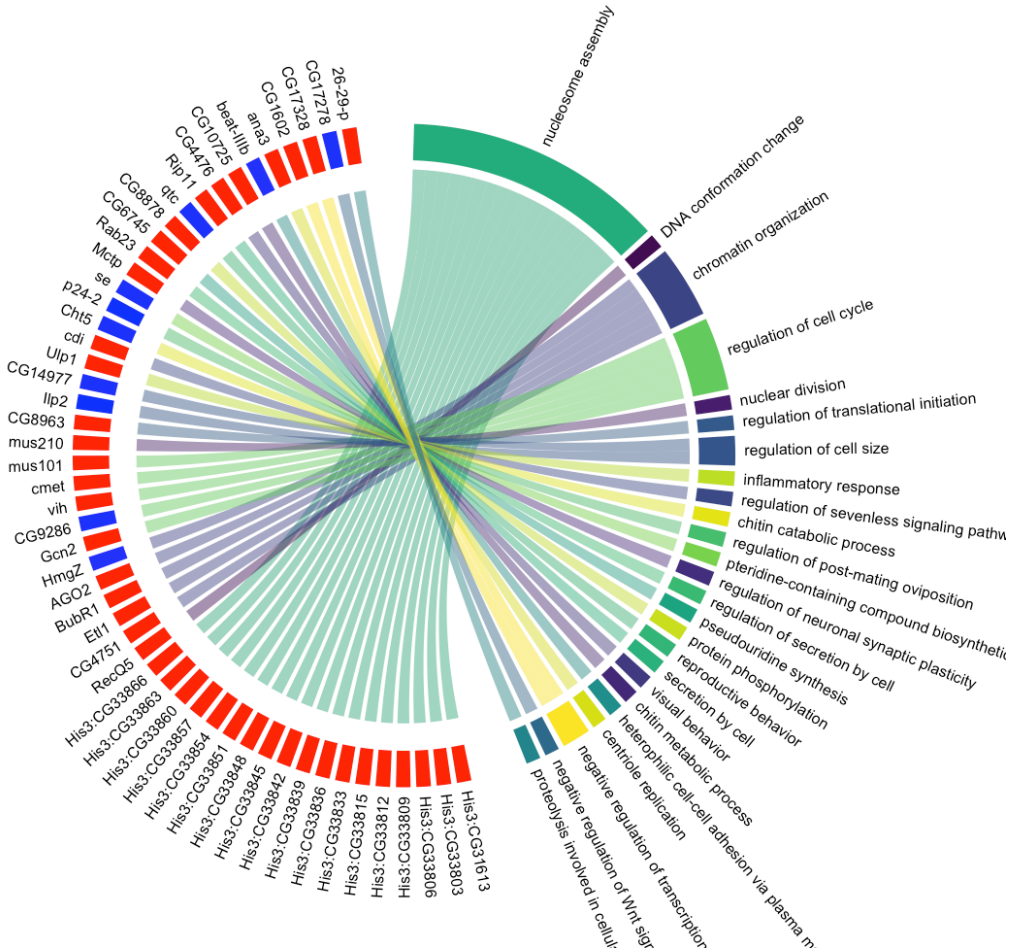

Figure S5. Circle plot of RpL24-like mutants indicating the association between differentially expressed genes inside the "RpL24-like" gene cluster and their associated GO terms. Associations between individual genes and their terms are indicated with ribbons. Genes upregulated in the RpL24-like module are represented in red and those downregulated in blue.

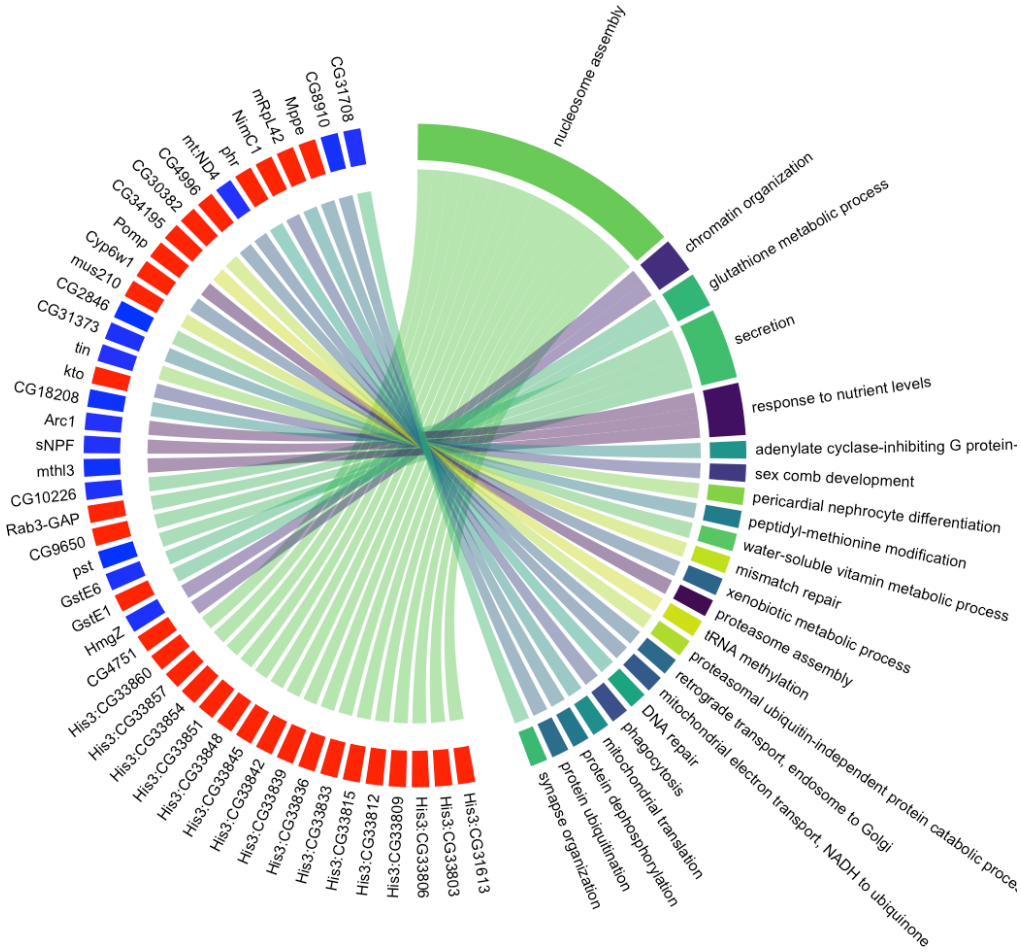

Figure S6. Circle plot of RpL30 mutants indicating the association between differentially expressed genes inside the "RpL30" gene cluster and their associated GO terms. Associations between individual genes and their terms are indicated with ribbons. Genes upregulated in the RpL30 module are represented in red and those downregulated in blue.

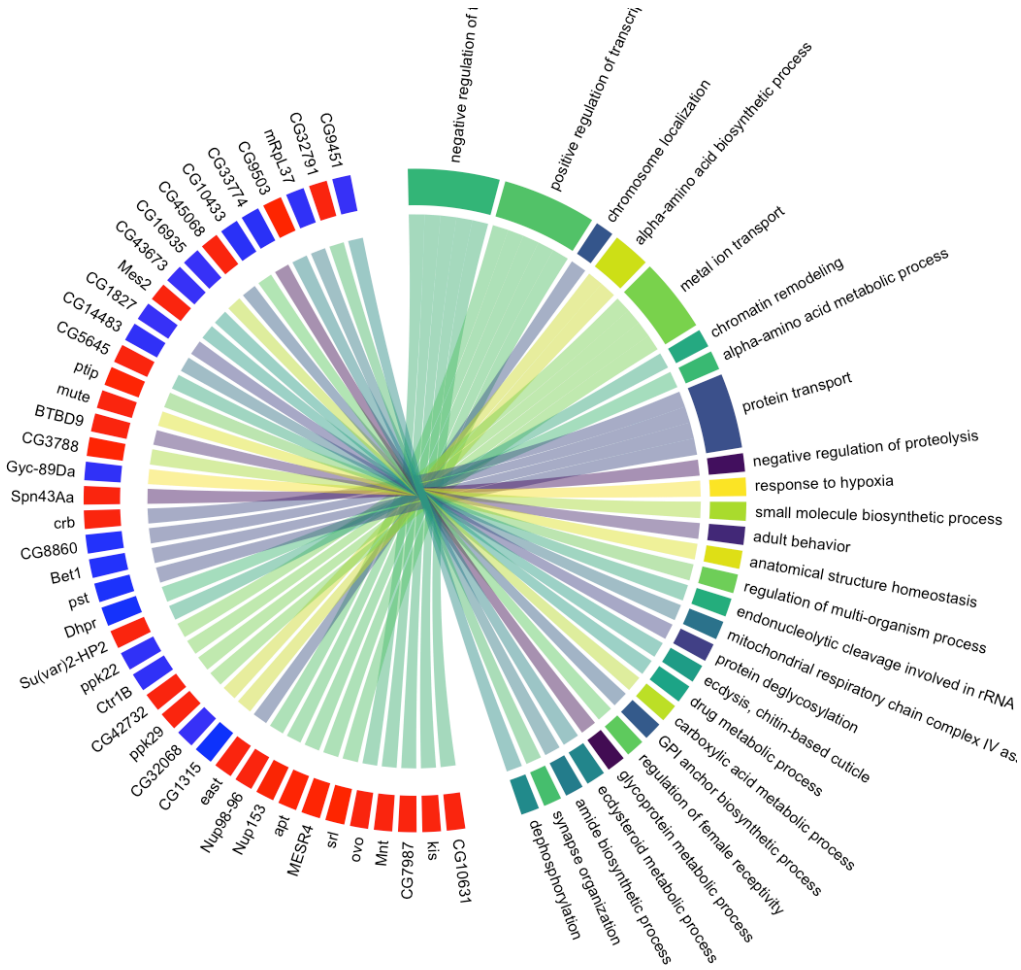

Figure S7 - Circle plot of RpL19 mutants indicating the association between differentially expressed genes inside the "RpL19" gene cluster and their associated GO terms. The association between individual genes and their GO terms is indicated via a ribbon. Upregulated genes in the RpL19 module are represented in red and downregulated genes in blue.